

1 Multidimensional mapping of root responses to soil

2 environmental cues using a luminescence-based GLO-Roots:

3 an imaging systemplatform enabling multidimensional

4 characterization of soil-grown roots systems

Rubén Rellán-Álvarez^{1, 9}, Guillaume Lobet², Heike Lindner^{1, 8}, Pierre-Luc Pradier^{1, 8, 10},
Jose Sebastian^{1, 8}, Muh-Ching Yee¹, Jose Sebastian¹, Yu Geng^{1, 7}, Charlotte Trontin¹,
Therese LaRue³, Amanda Schrager-Lavelle⁴, Cara H. Haney⁵, Rita Nieu⁶, Julin Maloof⁴,
John P. Vogel⁷, José R. Dinneny^{1, 12}

⁹ ¹ Department of Plant Biology, Carnegie Institution for Science, Stanford, CA, USA.

¹⁰ ² PhytoSystems, University of Liège, Liège, Belgium.

¹¹ ³ Department of Biology, Stanford University, Stanford, CA, USA.

¹² ⁴ Department of Plant Biology, UC Davis, Davis, CA, USA.

¹³ ⁵ Harvard Medical School/Massachusetts General Hospital, Department of Genetics/Harvard

¹⁴ Department of Molecular Biology Boston, MA, USA

¹⁵ ⁶ USDA Western Regional Research Center, Albany, CA, USA

¹⁶ ⁷ DOE Joint Genome Institute, Walnut Creek, CA, USA

¹⁷ ⁸ These authors contributed equally

¹⁸ ⁹ Present address: Unidad Laboratorio Nacional de Genómica Avanzada para la
Biodiversidad (Langebio), CINVESTAV-Irapuato, Unidad de Genómica Avanzada,
Centro de Investigación y de Estudios Avanzados del Instituto Politécnico Nacional
(CINVESTAV-IPN), Irapuato, Guanajuato, México –

²² ¹⁰ Present address: Boyce Thompson Institute for Plant Research/USDA, Ithaca, NY, USA.

²³ ¹¹ Present address: Energy Biosciences Institute, UC, Berkeley, CA, USA

²⁴ ¹² Corresponding author

²⁵ **Author contributions:**

²⁶ RR-A: Conception, design and development of the growth and imaging system and Arabidopsis transgenic lines; acquisition, analysis and interpretation of data; drafting and revising the article.

²⁹ GL: Development of the GLO-RIA image analysis plugin, analysis and interpretation of data, drafting and revising the article.

³¹ HL: Acquisition of data, development of the tomato growth and imaging setup.

³² P-LP: Acquisition of data, analysis and interpretation of data

³³ **MCY: Development of Arabidopsis and Brachypodium transgenic lines.**

³⁴ JS: Development of Brachypodium transgenic lines, acquisition and analysis of Brachypodium [Arabidopsis and tomato](#) data.

³⁶ **MCY: Development of Arabidopsis and Brachypodium transgenic lines.**

³⁷ YG: Development of Arabidopsis transgenic lines.

³⁸ CT: Acquisition and analysis of the QPCR data

³⁹ TL: Acquisition and analysis of the QPCR data

⁴⁰ AS-L: Contributed the unpublished dual-color tomato line.

⁴¹ CH: Contributed the unpublished *Pseudomonas fluorescens* CH267-lux strain.

⁴² RN: Contribution to the development of the Brachypodium transgenic line.

⁴³ JM: Contributed the unpublished dual-color tomato line.

⁴⁴ JPV: Contribution to the development of the Brachypodium transgenic line.

⁴⁵ JRD: Conception, design and development of the growth and imaging system and Arabidopsis transgenic lines; acquisition, analysis and interpretation of data; drafting and revising the article.

⁴⁸ All authors read and approve the final version of the manuscript.

⁴⁹ Abstract

⁵⁰ Root systems develop different root types that individually sense cues from their local
⁵¹ environment and integrate ~~them~~ this information with systemic signals. This complex multi-
⁵² dimensional amalgam of inputs ~~leads to~~ enables continuous adjustment of root growth rates,
⁵³ direction and metabolic activity ~~to~~ that define a dynamic physical network. Current methods
⁵⁴ for analyzing root biology balance physiological relevance with imaging capability. To bridge
⁵⁵ this divide, we developed an integrated imaging system called Growth and Luminescence
⁵⁶ Observatory for Roots (GLO-Roots) that uses luminescence-based reporters to enable studies
⁵⁷ of root architecture and gene expression patterns in soil-grown, light-shielded roots. We have
⁵⁸ developed image analysis algorithms that allow the spatial integration of soil properties such
⁵⁹ as soil moisture with root traits. We propose GLO-Roots as a system that has great utility in
⁶⁰ ~~both~~ presenting environmental stimuli to roots in ways that evoke natural adaptive responses ~~,~~
⁶¹ and in providing tools for ~~developing a~~ studying the multi-dimensional ~~understanding~~ nature
⁶² of such processes.

⁶³ Introduction

⁶⁴ Plant roots are three-dimensional assemblies of cells that coordinately monitor and acclimate
⁶⁵ to soil environmental change by altering physiological and developmental processes through
⁶⁶ cell-type and organ-specific regulatory mechanisms^{1,2}. Soil comprises a complex distribution
⁶⁷ of particles of different size, composition and physical properties, airspaces, variation in
⁶⁸ nutrient availability and microbial diversity^{3,4}. These physical, chemical and biological
⁶⁹ properties of soil can vary on spatial scales of meters to microns, and on temporal scales
⁷⁰ ranging from seasonal change to seconds. Root tips ~~likely~~ monitor this environment through
⁷¹ locally and systemically acting sensory mechanisms^{5,6}.

⁷² The architecture of the root system determines the volume of soil where resources can be

73 accessed by the plant (rhizosphere). Because the physical and chemical properties of these
74 resources vary, their distribution in the soil column is distinct⁴. Water and water-soluble
75 nutrients such as nitrogen or manganese move through the soil by bulk flow and tend to
76 accumulate deeper in the soil profile as a consequence of gravity⁷, while other nutrients
77 such as phosphorus and potassium, which tightly bind to soil particles, tend to accumulate
78 in the upper layers of soil where decomposition of organic matter replenishes their supply⁷.
79 Developmental processes that affect root growth rate and direction will influence the
80 efficiency with which specific resources are captured from the rhizosphere. Root systems
81 optimized to capture one resource may be inefficient for another.

82 Root architecture is and is under both environmental and genetic control; plasticity.
83 Plasticity in growth parameters allows the plant to adjust its form to suit a particular
84 soil. Lateral roots, which usually make up the majority of the total root system, often
85 grow at an angle divergent from the gravity vector. This gravity set-point angle (GSA) is
86 controlled by auxin biosynthesis and signaling and can be regulated by developmental age
87 and root type⁸⁷. Recent cloning of the *DRO1* Quantitative Trait Locus (QTL) demonstrates
88 that natural genetic variation is a powerful tool for uncovering such control mechanisms⁹⁸.
89 Specific root ideotypes (idealized phenotypes) have been proposed to be optimal for acquisition
90 of water and nitrogen, which are distinct from ideotypes for low phosphorus. Based on
91 computational modeling and field studies, the “steep, deep and cheap” ideotype proposed
92 by Lynch and colleagues may provide advantages to the plant for capturing water and
93 nitrogen elements like nitrogen that are water soluble and therefore tend to move in the soil
94 column with water. This ideotype consists of highly gravitropic, vertically oriented roots that
95 grow deep in the soil column and develop large amounts of aerenchyma, which reduces the
96 overall metabolic cost of the root system³. Low phosphorus conditions, on the other hand,
97 Other nutrients, like phosphorus, which have limited water solubility and are tightly bound
98 to organic matter, usually accumulate in the top layers of soil and favor roots systems that
99 are more highly branched and shallow. The low-phosphorus ideotype effectively increases
100 root exploration at the top layers of soil³. Modeling of root system variables shows that

101 optimum architecture for nitrogen and phosphorus uptake are not the same¹⁰⁹ and suggests
102 tradeoffs that may affect the evolution of root architecture as a population adapts to a
103 particular environmental niche.

104 Clearly, understanding the architecture of root systems and how environmental conditions
105 alter root developmental programs is important for understanding adaptive mechanisms of plants and for identifying the molecular-genetic basis for different response programs. **Experimental methods for studying root architecture can be divided into two general categories that each represent compromises in either physiological relevance or versatility.**

109 **Growth of plants in gels such as agar or gellan gum provides a transparent support medium which allows immediate visual access to roots. Simple devices can be used to capture macroscopic images of roots¹¹ or confocal microscopy can be implemented for studying cell-scale processes. Gel media allows exact control over the concentration of nutrients¹² or stressful components¹³ and fluorescent reporters can be deployed to track the activity of genes, proteins or metabolites. This approach has been extensively used in the model plant *Arabidopsis* and has allowed for the discovery of many fundamental processes. Root system architecture studies and high resolution time-scale analysis of root growth are easily performed when used in combination with automatic time-lapse imaging^{14,15}. Variations of this approach have been used in other species to study root system architecture in three dimensions^{???}. Most often, in gel-based media systems, roots are exposed to light¹⁷ while shoots are enclosed in a high humidity head space that does not permit transpiration from the leaf surface. Media is typically axenic and with highly artificial levels and distributions of nutrients. Gas exchange between the root and the media is limited and might lead to hypoxia or ethylene buildup. *In vitro* growth conditions are also limited in the length of time plant growth can be supported. Typical studies examine roots during the first 1-2 weeks after seed germination whereas the life-cycle of *Arabidopsis* lasts for two months or longer, depending on the accession. Moreover, the relevance of root architectural phenotypes that are highly influenced by light raises concerns regarding the importance of any loci identified using *in vitro* conditions¹⁷. Due to these limitations, studying processes that involve whole plant**

129 sensing of environmental cues such as water or nutrient availability must be viewed with
130 caution.

131 A less transparent but more physiologically relevant medium to study root growth is
132 soil. Plants are grown in soil in the field or in pots. Root imaging can be achieved by
133 several means, from uprooting plants using a shoveling pipeline^{18,19} to growth of roots
134 in transparent pots or in rhizotrons²⁰, literally “root devices” that are constructed to
135 allow visualization of roots in proximity to a transparent glass or plastic plate. More
136 recently, the use of techniques such as X-ray micro computed tomography has opened the
137 possibility of *in situ* characterization of root architecture, water content and soil particles
138 in 3-D^{5,21}. Such methods are limited due to their relative cost, the volume of soil that can
139 be imaged, the current limit in resolution and the inability to monitor gene expression or
140 other molecular processes.

141 Roots systems have additional In addition, roots systems have complexity beyond their
142 architecture that needs to be incorporated into our understanding of plant-environment inter-
143 actions. Primary and lateral roots exhibit different stress response programs in *Arabidopsis*²
144 and may play specialized roles in water and nutrient uptake. Thus, it is important to
145 develop methods that allow for a multidimensional characterization of the root system that
146 includes growth, signaling, and interactions with other organisms. Furthermore, physiological
147 parameters that affect whole plant responses to the environment, such as transpiration, are
148 likely integrated into such processes, thus requiring a more holistic approach to studies of
149 root function.

150 Based on these considerations we have developed a new root imaging platform, Growth and
151 Luminescence Observatory for Roots (GLO-Roots), which allows root architecture and gene
152 expression to be studied in soil-grown plants. GLO-Roots is an integrated system composed
153 of custom growth vessels, luminescent reporters and imaging systems. We use rhizotrons
154 that have soil volumes equivalent to small pots and support growth of *Arabidopsis* from
155 germination to senescence. To visualize roots, we designed plant-codon optimized luciferase
156 reporters that emit light of different wavelengths. To visualize reporter expression, plants

157 are watered with a dilute luciferin solution and imaged afterwards. We have ~~designed~~built
158 a custom luminescence imaging system that automatically captures images of rhizotrons
159 held vertically. The signal from each reporter is distinguished using band-pass filters held
160 in a motorized filter wheel, which enables automated acquisition of images from plants
161 expressing both structural and environmentally and developmentally responsive reporters.
162 We have also developed GLO-RIA (GLO-Roots Image Analysis) ~~software~~, an ImageJ???
163 plugin that allows for automated determination of root system area, convex hull, depth,
164 width and directionality, which quantifies the angle of root segments with respect to gravity.
165 GLO-RIA is also able to relate root system parameters to local root-associated variables
166 such as reporter expression intensity ~~or and~~ soil-moisture content.
167 Overall GLO-Roots has great utility in presenting environmental stimuli to roots in physi-
168 logically relevant ways and provides tools for characterizing responses to such stimuli at
169 the molecular level ~~whole roots of adult plants~~in whole adult root systems over broad time
170 scales.

171 **Box 1.**

172 All resources for GLO-Roots, including the original raw data used in the manuscript, sample
173 images, GLO-RIA user manual, the latest software updates and the source code, can be
174 found at: <https://dinnenylab.wordpress.com/glo-roots/>

175 **Results**

176 We have developed an integrated platform for growing, imaging and analyzing root growth
177 that provides advances in physiological relevance and retains the ability to visualize aspects
178 of root biology beyond structure.

179 **THE GLO-ROOTS PLATFORM**The GLO-Roots platform

180 GLO-Roots is comprised of four parts: i) growth vessels called rhizotrons that allow plant
181 growth in soil and root imaging; ii) luminescent reporters that allow various aspects of root
182 biology to be tracked in living plants; iii) luminescence imaging GLO1 luminescence-imaging
183 system designed to automatically image rhizotrons; iv) GLO-RIA, an image analysis suite
184 designed to quantify root systems imaged using GLO-Roots.

185 **Plant growth system** GLO-Roots utilizes custom designed growth vessels classically
186 known as rhizotrons, which hold a thin volume of soil between two sheets of polycarbonate
187 plastic. Acrylic spacers provide a 2-mm space in which standard peat-based potting mix is
188 added. Black vinyl sheets protect roots from light and rubber U-channels clamp the rhizotron
189 materials together. Plastic racks hold the rhizotrons vertically and further protect the roots
190 from light. Rhizotrons and rack are placed in a black tub and about 2 cm of water are
191 addedto, to a depth of about 2 cm, at the bottom to maintain moisture in the rhizotrons
192 during plant growth. The volume of soil in the rhizotrons (100 cm^3) is similar to small pots
193 commonly used for Arabidopsis growth and supports growth of Arabidopsis throughout its
194 throughout the entire life cycle (Fig 1A-C and Supplement 1).

195 While the 2 mm depth of the soil sheet is 20 times the average diameter of the Arabidopsis
196 root tip (approximately 100 microns), we wanted to evaluate whether rhizotron-grown plants
197 exhibited any obvious stress as a consequence of physical constriction. We compared traits
198 of plants growing in vessels that hold similar volumes of soil but in different geometric
199 shapes. No significant differences in shoot area were observed between the three systems
200 (not shown). The number of lateral roots was significantly lower in pot and cylinder-grown
201 plants compared to rhizotron-grown plants (Fig 1F) whereas primary root length of rhizotron
202 and cylinder-grown plants was similar and significantly greater than for pot-grown plants
203 (Fig 1G). Thus, these data do not support the hypothesis that rhizotron-grown plants
204 experience physical constriction greater than other vessels holding the same volume of soil.

205

206 We next compared root systems grown on the surface of agar or in soil. Shoot weight and
207 primary root length were significantly reduced for gel-grown plants compared to rhizotron-
208 or pot-grown plants suggesting significant differences in the biology of plants grown under
209 these conditions (Fig 1H-I). To determine how soil-grown and gel-grown root systems might
210 differ in their biology To determine how the biology of plants grown in rhizotrons compares
211 to other standard growth systems, we utilized high-throughput qRT-PCR to study a
212 panel how these conditions affect expression of 77 genes marker genes in root and shoot
213 samples. These genes were curated from the literature that and belong to a wide array
214 of biological pathways including nutrient acquisition and hormone and light response to
215 and abiotic stress. Whole roots and shoot samples were collected at the end of the light
216 and dark cycles (periods (Long-day conditions: 16 hour light, 8 hours dark) from plants
217 grown in rhizotrons, pots, and petri dishes with two different media recipes compositions
218 (1X Murashige and Skoog basal salts (MS), 1% sucrose or 0.25X MS, no sucrose).
219 Principal component analysis of the gene expression values showed a clear separation of
220 soil and gel-grown root systems in the first two principal components with a clear overlap
221 between rhizotron and pot-grown root system samples (Fig 1D). Significant differences in
222 the first principal components (Figure 1-figure supplement 1A). In roots grown on gel-based
223 media, we observed enhanced expression of genes associated with flavonoid biosynthesis
224 (light-regulated pathways (flavonoid biosynthesis: *FLAVINOL SYNTHASE1*, *FLS1*)
225 and phosphorus nutrition (, *CHALCONE SYNTHASE*, *CHS* and photosynthesis: *LOW*
226 *PHOSPHATE RESPONSE1**RUBISCO SUBUNITS1A*, *RBCS1A*, *LPR1**CYCLOPHILIN*
227 *38*, *PHOSPHATE STARVATION RESPONSE1*, *PHR1**CYP38*) were observed (Fig 1E)
228 Flavonoids contribute to anthocyanin biosynthesis, which are UV protectants. Importantly,
229 however, flavonoids have also been implicated in the regulation of root developmental
230 traits²², suggesting that light induction of these pathways in, which is expected due to
231 the exposure of gel-grown roots could influence such processes. *SUPER ROOT1 (SUR1)*,
232 which promotes biosynthesis of the anti-microbial metabolite indole glucosinolate, was
233 significantly associated with soil-grown roots, suggesting the non-sterile soil environment
234 may induce to light. In addition, genes associated with defense. *XYLOGLUCAN*

235 *ENDOTRANSGLUCOSYLASE/HYDROLASE17* (phosphorus nutrition (*XTH17*) and
236 *TOUCH4* (*TCH4*), both of which respond to touch stimuli, were expressed more highly) *LOW*
237 *PHOSPHATE RESPONSE1, LPR1, PHOSPHATE STARVATION RESPONSE1, PHR1*)
238 were (Figure 1-figure table supplement 1) less expressed in soil-grown roots consistent
239 with the presence of physical barriers in soil while growth in gel may present fewer
240 obstructions, suggesting differences in nutrient availability between the different growth
241 systems. Interestingly, shoot samples were not clearly distinguished by growth media
242 and, instead, time of day had a greater effect (Fig. 1E and Figure 1 Supplement 1Figure
243 1-Supplement 2). These data suggest root systems may be particularly sensitive to media
244 conditions –and indicate that rhizotron-grown root systems more closely approximate the
245 biology of pot-grown plants than standard gel-based media. Shoot weight and primary
246 root length were significantly reduced for gel-grown plants compared to rhizotron- or
247 pot-grown plants suggesting significant differences in the biology of plants grown under
248 these conditions (Figure 1-figure supplement 1B-C). While the 2 mm depth of the soil
249 sheet is 10 to 20 times the average diameter of an Arabidopsis root (between 100-200
250 microns??), we evaluated whether rhizotron-grown plants exhibited any obvious stress
251 as a consequence of physical constriction. We compared traits of plants growing in
252 vessels that hold similar volumes of soil but in different volumetric shapes. The number
253 of lateral roots was significantly lower in pot and cylinder-grown plants compared to
254 rhizotron-grown plants (Figure 1-figure supplement 1D) whereas primary root length of
255 rhizotron and cylinder-grown plants was significantly greater than pot-grown plants (Figure
256 1-figure supplement 1E). No significant differences in shoot area were observed between the
257 three systems (Figure 1-figure supplement 1-data). Thus, these data do not support the
258 hypothesis that rhizotron-grown plants experience physical constriction greater than other
259 vessels holding the same volume of soil.

260 **Generation of transgenic plants expressing different luciferases** Arabidopsis roots
261 cannot be easily distinguished from soil using brightfield imaging due to their
262 thinness and translucency (Figure 1-figure supplement 3); thus, reporter genes are needed to

enhance the contrast between the root and their environment. Luciferase is an ideal reporter to visualize roots: 1) unlike fluorescent reporters, luciferase does not require high-intensity excitation light, which could influence root growth, 2) peat-based soil ([a type of histosol](#)) exhibits no autoluminescence but does autofluoresce at certain excitation wavelengths similar to GFP ([data not shown](#)[Figure 1-figure supplement 3](#)), 3) while GFP is very stable, and thus not as suitable for imaging dynamic transcriptional events, the luciferase enzyme is inactivated after catabolism of luciferin, making it ideal for studying processes such as environmental responses. A considerable number of luciferases have been developed that emit light spanning different regions of the visible spectrum, but their utilization has been limited to studies in animals (Table 1).

To determine the efficacy of using luciferase to visualize roots in soil, we codon optimized sequences of *PpyRe8PpyRE8*, *CBGRed*, *LUC2*, and *CBG99* for Arabidopsis expression. In addition, nanoLUC and venus-LUC²³¹⁰ were utilized. Constitutive luciferase expression was driven in plants using the [UBIQUITIN 10 \(UBQ10\)](#) or [ACTIN2 \(ACT2\)](#) promoter using vectors assembled through a [Golden Gate cloning system](#)[Golden-Gate cloning system](#)²⁴¹¹. Plants homozygous for a single locus T-DNA insertion were evaluated for in vivo emission spectra and luminescence intensity (Fig [2A1D](#)). All the evaluated luciferases use D-luciferin as a substrate facilitating the simultaneous imaging of different luciferases except nanoLUC, which uses a proprietary substrate [furimazine](#)¹². In general, luciferases with red-shifted emission spectra were less intense than the green-shifted luciferases (Fig [2A1D](#)). LUC2o showed an emission maximum at 580 nm and a minor peak at 620 nm while CBG99o lacks the minor peak.

[Continuous addition of luciferin did not have any significant effect on shoot weight or primary root length \(Figure 1-figure supplement 4\). After luciferin addition, luminescence signal could be reliably detected in root systems for up to 10 days, depending on the developmental state of the plant.](#)

289 **GLO1: a semi-automated luminescence imaging system for rhizotrons** Lumines-
290 cence imaging systems commercially available for biomedical research are usually optimized
291 for imaging horizontally held specimens or samples in microtiter plates. Placing rhizotrons
292 in this position would induce a gravitropic response in plants. Working with Bioimaging
293 Solutions (San Diego, CA) we designed and built a luminescence imaging system optimized
294 for rhizotron-grown plants. GLO1 (Growth and Luminescence Observatory 1) uses two
295 back-thinned CCD cameras (Princeton Instruments, USA) to capture partially-overlapping
296 images of rhizotrons while a motorized stage automatically rotates the rhizotron to capture
297 images of both sides (Fig 2B1E). A composite image is generated from the images captured
298 of each side; Fig 2C-1F shows that approximately half of the root system is revealed on
299 each side with few roots being visible on both sides. ~~This result suggests that the depth of~~
300 ~~soil in the rhizotron is sufficient to block visibility of roots beyond the mid-point of the soil~~
301 ~~sheet but not so thick that a continuous root system is difficult to reconstruct~~ Apparently,
302 ~~the soil sheet is thick enough to block portions of the root system but thin enough to ensure~~
303 ~~its continuous structure can be compiled from opposite face views.~~ We tested the ability
304 of GLO1-generated images to reveal complete root systems by manually quantifying the
305 number of lateral roots in excavated root systems of 8 different plants and testing these
306 results against estimates of lateral root number from images of the same plants visually
307 inspected by 4 different persons. These comparisons revealed good correlation ($(R^2 = 0.974)$)
308 between actual lateral root counts and image-based estimation, indicating GLO1-generated
309 root images provide an accurate representation of the in soil-soil root system.

310 ~~Continuous addition of luciferin did not have any significant effect on shoot weight or primary~~
311 ~~root length (Figure 2 Supplement 1). After luciferin addition, luminescence signal could be~~
312 ~~reliably detected in root systems for up to 10 days, depending on the developmental state~~
313 ~~of the plant.~~

314 **GLO-RIA: GLO-Roots Image Analysis** Current image analysis algorithms are
315 ~~optimized for roots that are continuously visible, since they are designed to work with~~
316 ~~images of roots grown in transparent media or on paper. Root systems visualized with~~

317 GLO-Roots, however, often contain breaks in the continuity of primary and lateral root
318 signal, which likely results from soil particles obscuring the object. We developed a set of
319 image analysis algorithms that were well suited for the complex root systems ~~which that~~
320 GLO-Roots is able to capture. GLO-RIA (Growth and Luminescence Observatory Root
321 Image Analysis) is an ImageJ plugin ~~that can automatically identify the perimeter of the~~
322 ~~root divided in two modules. The first module (RootSystem) performs four different types~~
323 ~~of analysis: i) a local analysis that detects all root particles in the image and computes their~~
324 ~~position, length and direction; ii) the global analysis performs a root system level analysis~~
325 ~~and computes the total visible surface, convex hull, width and depth; iii) the shape analysis~~
326 ~~uses Elliptic Fourier Descriptors or pseudo-landmarks similarly to RootScape^{???} to perform~~
327 ~~a shape analysis on the root system iv) the directionality analysis computes the mean~~
328 ~~direction of root particles in a root system (either on the full image or by a user-defined~~
329 ~~region of interest in the image). These four analysis methods are fully automated by default,~~
330 ~~but can be manually adjusted if needed. The second module of GLO-RIA (RootReporter)~~
331 ~~was specifically designed for the analysis of multi-layered images such as combinations of~~
332 ~~gene reporter, root structure and soil moisture. Shortly, the plugin works as follows: i)~~
333 ~~detection of the gene reporters and the structure reporters in their respective images; ii) if~~
334 ~~needed, a manual correction can be performed to correct the automated detection; iii) gene~~
335 ~~reporters are linked with the soil water content and the structure reporters, based on their~~
336 ~~proximity; iv) gene reporter intensity (either absolute or normalized using the structural~~
337 ~~reporter) is computed; v) all data are exported and saved to a RSML datafile¹³. Gene~~
338 ~~and structure reporters can be followed across different time and space points. Using an~~
339 ~~object oriented approach, great care has been taken to facilitate the user interactions on~~
340 ~~the different images to streamline the analysis process. Table 2 shows a list of root system~~
341 ~~and quantify aspects of root system geometry derived from this outline. We have also used~~
342 ~~a that utilizes a sobel filter to identify edges in an image and quantifies the proportion of~~
343 ~~quadrants that exhibit a bias in angle of such edges with respect to the axes of the image.~~
344 ~~Similar algorithms have been used to quantify dynamic changes in the plant cytoskeleton²⁵.~~
345 ~~Directionality measurements can rapidly capture lateral root angles at the whole root~~

346 system level without the need to define individual roots features extracted using GLO-RIA.
347 GLO-RIA does not currently have the ability to reconstruct the root architecture in itself
348 (topological links between roots). This is a challenge for analyzing images captured by
349 GLO-Roots since soil particles cause disruption of root segments.

350 **Continuous imaging of root growth**

351 The size of our rhizotrons enables undisturbed root system development (before roots reach
352 the sides or the bottom of the rhizotron) for about 21-23 days for the Col-0 accession growing
353 under long day conditions ([Figure 2](#)); however root traits besides width and depth can
354 continue to be observed until senescence of the plant such as directionality can be observed
355 through later stages of plant development. See [35 DAS root system and directionality in](#)
356 [Figure 2A-B](#). An example of a time series spanning 11 to 21 days after sowing (DAS) of Col-0
357 roots expressing *ProUBQ10:LUC2o* is shown in Fig [3A-2A](#) and [Video 1](#) with a color-coded
358 time projection shown in Fig [3B2C](#). Directionality analysis (Fig [3C2B](#)) shows a progressive
359 change in root system angles from 0 ° (vertical) to 45 ° as lateral roots take over as the
360 predominant root type. Figure [3D-2D](#) shows the evolution over time of several root traits
361 that can be automatically captured by GLO-RIA (depth, width, area) and others that can be
362 were manually quantified (primary root growth rate or number of lateral roots per primary
363 root length).

364 **Root system architecture of different *Arabidopsis* accessions.**

365 The study of natural variation for root system architecture and root traits is a powerful
366 approach for understanding adaptive strategies plants use to cope with environmental change
367 and for identifying the genetic basis for such differences. In *Arabidopsis*, Quantitative Trait
368 Locus (QTL) and Genome-Wide Association Studies (GWAS) have led to the identification
369 of genes affecting root development²⁶. However, traits are usually measured in seedlings
370 less than 2 week old. Selective pressures that affect allele frequencies in a population likely
371 act on genes that affect root system traits at later stages of the plant life cycle, as well. As

372 a proof of concept to estimate the utility of our root imaging system to phenotype adult
373 root system traits, we transformed a small set of accessions (Bay-0, Col-0 and Sha) with
374 the *ProUBQ10:LUC2o* reporter and quantified RSA at 22 DAS (~~days after sowing~~Fig 3A-C).
375 GLO-RIA analysis of these root systems identified several root traits that distinguish Col-0,
376 Bay-0 and Sha(Fig 4. Directionality analysis revealed an abundance of steep-angle regions in
377 the root system of Bay while Sha showed an abundance of shallow-angled regions and Col-0
378 was intermediate (Fig 3D)). Bay-0 shows the deepest and narrowest root system leading to
379 the highest depth/width ratio while Sha has the widest root system ~~, Directionality analysis~~
380 ~~revealed an abundance of steep-angle regions in the root system of Bay while Sha showed~~
381 ~~an abundance of shallow-angled regions and Col-0 was intermediate (Fig 4D(Fig 3E))~~. Other
382 ~~root traits such as root system area and the vertical center of mass also showed significant~~
383 ~~differences (Figure 3-figure supplement 1B)~~. Broad sense heritability values for depth (96.3),
384 area (92.0), depth/width (97.8), width (95.7) and vertical center of mass (95.0) were all
385 higher than 90%.—

386 **GLO-Roots for *Brachypodium* and Tomato**

387 To examine the general applicability of
388 To capture the richness of root architecture shape, we used GLO-RIA to extract
389 pseudo-landmarks describing the shape of the root system (see Materials and Methods
390 for more details) and performed PCA analysis. The first principal component captures
391 differences in the GLO-Roots system for other species we introduced LUC2o-expressing
392 reporters into the model grass *Brachypodium distachyon* and the crop plant *Lycopersicon*
393 *esculentum* (tomato). *Brachypodium* is well suited to the GLO-Root system because, like
394 *Arabidopsis*, its small size allows mature root systems to be studied in relatively small soil
395 volumes^{27,28}. *LUC2o* driven by the *ZmUb1* promoter was introduced into *Brachypodium*
396 using the pANIC vector²⁹. *Brachypodium* roots showed a distinct architecture from
397 *Arabidopsis* marked by prolific development of secondary and tertiary lateral roots (Fig
398 5A). This is consistent with other studies that show that *Brachypodium* has a typical

399 grass root system²⁸. After 26–28 days of growth, shoot-derived crown roots initiated and
400 took over as the predominant part of the root system (not shown). Comparison of root
401 system development in rhizotrons with gel-based media showed that primary and lateral
402 root growth is more extensive in soil (Fig 5B). Interestingly, previous work has suggested
403 that auxin levels in *Brachypodium* roots is supra-optimal for growth³⁰. Our results suggest
404 that gel-based systems may lead to an imbalance in hormone signaling that causes slower
405 growth. distribution of widths along the vertical axis and separates Col-0 and Sha from
406 Bay-0 root systems. (Fig 3F). Bay-0 shows an homogenous distribution of widths along the
407 vertical axis while Sha and Col-0 are much wider at the top than bottom. PC2 seems to be
408 capturing a relationship between width at the top and total depth and separates Sha root
409 systems which are wide at the top and deep from Col-0 root systems which are wide but
410 not as deep as Sha. Shape information extracted from pseudo-landmarks can distinguish
411 the three different accession using PCA analysis (Fig 3G).

412 Tomato plants were transformed with *Pro35S:PPyRE8o* and *ProeDR5rev:LUC2* reporters
413 . The plants showed more rapid growth than *Arabidopsis* or *Brachypodium* and required
414 fertilizer to prevent obvious signs of stress (reduced growth, anthocyanin accumulation).
415 Root systems were imaged from 14 DAS plants. Roots showed less branching than for
416 *Arabidopsis* but showed many presumptive lateral root primordia marked by DR5 expression
417 (Fig 5C–D). These results show that the GLO-Roots method is widely applicable to study
418 root systems of plants and will likely be useful for studying root systems of other small to
419 medium sized model and crop plants.

420 **Spectrally distinct luciferases enable gene expression patterns, characterization**
421 **of root system interactions and microbial colonization.**

422 **Spectrally distinct luciferases enable characterization of root system**
423 **interactions, microbial colonization and gene expression patterns.**

424 Although root system architecture is usually studied in isolated plants, this is rarely the
425 ease in nature where plants compete for soil resources through root–root interactions.

Recent work in this area has suggested that roots from the same cultivar can grow without competition while roots from different cultivars avoid each other³¹. One of the major challenges in such studies is the ability to distinguish two overlapping root systems. We tested whether spectrally distinct luciferase reporters would enable additional information besides root architecture to be captured from root systems. Luciferase reporters have been commonly used to study gene expression and these resources can potentially be utilized to study such regulatory events in soil-grown roots. We transformed *ProACT2:PpyRE8o* into two well studied LUC reporter lines: the auxin response reporter line *ProDR5:LUC+*¹⁴ (Figure A-B) and the Reactive Oxygen Species (ROS) response reporter *ProZAT12:LUC*¹⁵ (Figure 4C-D). We implemented in GLO-RIA an algorithm that semi-automatically identifies gene reporter signal and associates this object to the corresponding root structure segment. A graphical representation of the results obtained with Root Reporter can be observed in Figure 4-figure supplement 1. Reporter intensity values along the first 5 mm of root tips can also be observed in Figure 4-figure supplement 2. We then took advantage of our ability to constitutively express two spectrally different luciferases and imaged the overlapping root systems of two Col-0 plants (one expressing *ProUBQ10:LUC2o* and the other *ProACT2:Ppy RE8o*) or one Col-0 plant (expressing *ProACT2:Ppy RE8o*) and one Sha plant (expressing *ProUBQ10:LUC2o*). While two root systems were distinguishable using this system (Figure 4-figure supplement 3); measurements of root system area did not reveal a significant effect on root growth when two plants were grown in the same rhizotron, compared to one; however, further studies are warranted (Figure 4-figure supplement 3). Images were captured using unfiltered light and a custom (76.5 mm diameter) band-pass filter (415 nm – 485 nm), which captured light emitted predominantly by LUC2o. By overlaying the images, we were able to distinguish the two overlapping root systems (Figure 6-Supplement 1). We compared root traits of plants grown together or in isolation but could not observe any significant differences between treatments. This was also observed when Col-0 was grown with the Sha accession. Further studies are warranted, however, as environmental conditions where resources are limited may lead to more competition.

The GLO-Roots system uses non-sterile growth conditions, which allows complex biotic

455 interactions that may affect responses to the environment. Bacteria themselves can be
456 engineered to express luminescent reporters through integration of the LUX operon, which
457 results in luminescence in the blue region of the spectrum and is thus compatible with the
458 plant-expressed luciferase isoforms we have tested. *Pseudomonas fluorescens* CH267³²¹⁶,
459 a natural Arabidopsis root commensal, was transformed with the bacterial LUX operon
460 and used to inoculate plants. Thirteen days after inoculation, we were able to observe
461 bacterial luminescence colocalizing with plant roots. *P. fluorescens* did not show an obvious
462 pattern of colonization at the root system scale level. As a proof-of-principle test of the
463 multi-dimensional capabilities of the GLO-Roots system we visualized both *LUC2o* and
464 *PPyRE8o* reporters in plants and the LUX reporter in bacteria in the same rhizotron (Figure
465 [64-figure supplement 4](#)).

466 ~~One of the major advantages of our system is that luciferase reporters have been commonly~~
467 ~~used to study gene expression and these resources can potentially be utilized to study these~~
468 ~~regulatory events in soil-grown roots. We transformed *ProACT2:PpyRE8o* into two well~~
469 ~~studied LUC reporter lines: the auxin activity reporter line *ProDR5:LUC*³³ (Figure 7A)~~
470 ~~and the ROS activity reporter *ProZAT12:LUC*³⁴ (Figure 7B). We implemented in GLO-RIA~~
471 ~~an algorithm that semi-automatically identifies gene reporter signal and associates this~~
472 ~~object to the corresponding root structure segment. These two associated variables can~~
473 ~~be tracked in time lapse experiments. Using the *ProACT2:PpyRE8o* and *ZAT12:LUC* line~~
474 ~~we tracked root tip associated changes in growth and reporter expression throughout the~~
475 ~~whole root system in response to a local application of a 1 M NaCl solution over 24 hours. As~~
476 ~~shown in , reporter activity declines rapidly at the site of salt application while growth and~~
477 ~~ZAT12 reporter activity becomes induced further away at later time points and correlates~~
478 ~~with a burst of growth in this part of the root system (Fig 7E-F).~~

479 [Adaptive changes in root system architecture under water deprivation,](#)
480 [phosphorus deficiency and light](#)

481 **ADAPTIVE RESPONSES TO SOIL-BASED ENVIRONMENTAL STIMULI**

482 **Phosphorus availability promotes shallow root systems** To examine To test the
483 utility of the GLO-Roots system to understand response of root systems to environmental
484 stimuli we tested the effects of phosphorus availability on RSA we used alumina particles
485 buffered with 100 μ M phosphate (P) to supply this macro-nutrient to the root. Alumina
486 particles bind and release inorganic phosphorus similarly to soil particles, thus providing a
487 physiologically relevant nutrient regime³⁵. Alumina particles lacking P, which would remove
488 P supplied by the peat-based soil, were used to simulate a P-deficient soil. Root and shoot
489 phenotypes of control and P-deficient plants at 22 (Fig 8A) and 27 (Fig 8B) DAS are shown.
490 Plants grown in low-P soil showed a significant increase in the width-depth ratio of the root
491 system compared to plants grown in P-replete soil, as determined using the automated root
492 system area finder in GLO-RIA (Fig 8). Plants under P deficiency showed an increase in
493 the ratio between root:shoot area (Figure 8C) and higher investment of resources in the
494 development of the root system at the expense of shoot growth (Figure 8D). Root systems
495 of control and P-deficient plants showed no significant differences in directionality at 22
496 DAS but at 27 DAS, roots were more horizontally oriented in P-deficient plants (Figure 8E).
497 The observed changes in root architecture are consistent with root system ideotypes that
498 improve phosphorus uptake efficiency.

499 **Light promotes root gravitropism through PHOTOTROPIN signaling** light and
500 conditions that mimic drought and nutritional deficiency. To examine the effects of light
501 exposure on the root system architecture, the black shields, which normally protect the
502 soil and roots from light, were removed from the top half of the rhizotron rhizotrons 10
503 DAS. Using directionality analysis we detected a significant increase in the steepness of
504 roots only in the light exposed region of the rhizotron, while the lower shielded region
505 showed no difference. (Fig 9A-B^{figure supplement 3A-B} and Fig 6^{figure supplement 4}).
506 Light can penetrate the top layers of soil³⁶¹⁷ and it has been proposed to have a role in
507 directing root growth (Figure 9^{supplement 1}) specially in dry soils³⁷¹⁸ through the
508 blue light receptor *phot1*. Root directionality was not significantly different between light
509 and dark-treated roots of the *phot1/2* double mutant suggesting that blue light perception is

510 necessary for this response (Fig 9B), which is consistent with previous studies^{37,38,18,19} (Fig
511 [6-figure supplement 3B-lower panel](#)). These data highlight the strong effects of light on root
512 system architecture^{47,20}, which GLO-Roots rhizotrons are able to mitigate.

513 **Adaptive changes in root system architecture under water deprivation.** Plants
514 grown in low-P soil showed a significant increase in the width-depth ratio of the root
515 system compared to plants grown in P-replete soil, as determined using the automated
516 root system area finder in GLO-RIA (Fig [6-figure supplement 2A-B](#)). Plants under P
517 deficiency showed an increase in the ratio between root-shoot area (Fig [6-figure supplement](#)
518 [2C](#)) and higher investment of resources in the development of the root system at the expense
519 of shoot growth (Fig [6-figure supplement 2D](#)). Root systems of control and P-deficient
520 plants showed no significant differences in directionality at 22 DAS but at 27 DAS, roots
521 were more horizontally oriented in P-deficient plants (Fig [6-figure supplement 2E](#)). The
522 observed changes in root architecture are consistent with root system ideotypes that improve
523 phosphorus uptake efficiency.

524 GLO-Roots ~~provides important advantages over gel-based systems~~ is especially well suited
525 for studying water-deficit (WD) responses. First, shoots are exposed to the atmosphere and
526 vapor pressure deficit (VPD) is maintained at levels that allow for transpiration of water
527 from the shoot. Second, ~~WD can be simulated in more realistic ways than in gel. Soil in soil~~
528 [in](#) rhizotrons is exposed to air at the top and dries basipetally (from the top-down); drying
529 soil increases the volume occupied by air and reduces contact of root with liquid water, all of
530 which are similar to changes in soil expected in the field during WD. Finally, as peat-based
531 soil dries, its optical properties change, allowing moisture content to be approximated from
532 bright-field images. We took advantage of the change in gray-scale pixel intensity to construct
533 a calibration curve (Figure [10-Supplement](#) [5-figure supplement 1](#)) that quantitatively relates
534 gray-scale pixel intensity to moisture content (Fig [10A](#)[5A](#)); water content can be color coded
535 in images with appropriate look up tables (Fig [10B](#)-[5B](#)). ~~Soil color was not affected by~~
536 [the presence or absence of roots \(Figure 5-figure supplement 2\)](#). Using this approach, water
537 content in a rhizotron can be mapped and visualized in 2D (Fig [10C-D](#)[5C-D](#)). In the example

538 shown, we can observe that a 22 DAS Bay-0 plant depleted soil-moisture content locally
539 around the the root system (Figure 10E~~5E~~).

540 We performed several trials to simulate WD in our growth system. Plants were germinated,
541 grown under control conditions then transferred to 29°C and standing water ~~was~~ removed from
542 the container holding the rhizotrons starting at either 9 DAS or 13 DAS. Elevated temperature
543 combined with water deficit is a common stress that modern crops varieties are poorly adapted
544 to, thus highlighting the importance of examining this combined treatment^{3921,4022}. Plants
545 were maintained in this WD regime until 22 DAS when luciferin solution was added and
546 the plants ~~were~~ imaged. At 13 DAS, lateral roots near the soil surface are already emerged
547 (Video 1, Figure 3A). After 2A) and 9 days of ~~water-deficit treatment~~, ~~lateral roots showed~~
548 ~~subsequent WD treatment caused lateral roots to show~~ an increase in gravitropism leading
549 to the development of a root system that ~~was deeper~~, ~~were deeper and~~ more vertically
550 oriented ~~and with more tertiary roots~~ (Fig 11A~~(Fig 6A)~~). Roots of Bay-0 plants showed
551 similar responses, though the extent of change was less pronounced since Bay-0 roots are
552 normally more vertically oriented (Fig 11B~~6B~~). Plants transferred at 9 DAS and grown for
553 13 days under WD showed less lateral root development in the top layer of soil (Fig 11E~~6E~~).
554 At this time point, lateral roots start to emerge (Video 1) and early drought may lead
555 to growth quiescence or senescence. Careful examination of roots in these regions showed
556 evidence of small lateral root primordia populating the primary root (Figure 6F). After 24
557 h of re-watering (Figure 6G) these lateral root primordia reinitiated growth (Figure 6H).
558 Time-lapse imaging of the water deficit response showed that changes in root growth
559 direction occurred ahead of the dry soil front Video 2. Using GLO-RIA we were able
560 correlate local water moisture contents with the orientation of root segments. With this
561 approach we observed that root segments in dryer areas of rhizotron grew at steeper root
562 angles (Figure 7) than roots in WW regions, though lateral root angle in wetter regions was
563 also affected. These data suggest that both local and systemic signaling is likely involved
564 in redirecting lateral roots deeper during the simulated drought treatments tested here.

565 We also grew plants under WD at control temperatures or under WW conditions at ~~high~~

566 elevated temperature to test the effects ~~water and temperature had of these individual~~
567 stresses on root architecture~~in isolation~~. We observed that both conditions were sufficient to
568 induce a change in root directionality indicating that the plant uses similar mechanisms to
569 avoid heat and water-deficit associated stresses (Figure 11-Supplement 6-figure supplement
570 1). We next asked which regulatory pathways controlled the observed changes in lateral root
571 directionality during simulated drought. Hydrotropism is a known environmental response
572 that directs root growth towards wet regions of soil. MIZ1 is an essential regulator of
573 hydrotropism; however ~~miz1~~ mutants had no significant effect on water deficit-induced
574 changes in root directionality, compared to wild type (Fig 11E6C), indicating that this
575 response was distinct from hydrotropism. Auxin is an important mediator of gravitropism
576 and auxin treatment causes lateral roots to grow more vertically⁸⁷. Consistent with this
577 role for auxin, mutant plants with loss of function in the auxin receptor TIR1, did not show
578 changes in the root system directionality between WW and WD conditions (Fig 11D6D).

579 Plants transferred at 9 DAS showed less lateral root development in the top layer of soil. (Fig
580 11E) At this time point, lateral roots start to emerge (See) and early drought may lead to
581 growth quiescence or senescence¹⁰⁰⁰¹⁰⁰⁰². Careful examination of roots in these regions
582 showed evidence of small lateral root primordia populating parent roots (Figure 11F). After
583 24 h of re-watering (Figure 11G) these lateral root primordia reinitiated growth (Figure
584 11H)

585 GLO-Roots for Brachypodium and Tomato.

586 Time-lapse imaging of the water deficit response showed that changes in root growth
587 direction occurred ahead of the dry soil front. Using GLO-RIA we were able correlate
588 water moisture contents with local orientation of the root segments. With this approach we
589 observed that root segments in drier areas of rhizotron grew at steeper root angles (Figure
590 12) than roots in growing in well watered regions, though lateral root angle in wetter regions
591 was also affected. These data suggest that local and systemic signaling is likely involved in
592 redirecting lateral roots deeper during the simulated drought treatments tested here.

593 **Discussion**

594 Organisms have evolved to acclimate to environmental change through adaptive responses.

595 Stressful environmental conditions can elicit tolerance mechanisms that allow the organism

596 to bear the negative effects of sub-optimal conditions while avoidance mechanisms provide

597 alternative routes for acquiring needed resources. Environmental stresses such as phosphate

598 deprivation or water deficit simulated in gel-based systems typically cause a reduction

599 in root growth, suggesting that To examine the general applicability of the plant is

600 preserving resources to ensure survival. Interestingly, simulation of these same stresses

601 using the soil-based GLO-Roots system was able to elicit changes in root growth that

602 are anticipated to provide a mechanism to avoid stress system for other species, we

603 introduced LUC2o-expressing reporters into the model grass *Brachypodium distachyon* and

604 the crop plant *Lycopersicon esculentum* (tomato). *Brachypodium* is well suited to the

605 GLO-Root system because, like *Arabidopsis*, its small size allows mature root systems to

606 be studied in relatively small soil volumes^{1000100023,24}. *LUC2o* driven by the *ZmUb1*

607 promoter was introduced into *Brachypodium* using the pANIC vector²⁵. *Brachypodium*

608 roots showed a distinct architecture from *Arabidopsis* marked by prolific development of

609 secondary and tertiary lateral roots (Fig 8A). This is consistent with other studies that

610 show that *Brachypodium* has a typical grass root system²⁴. Comparison of root system

611 development in rhizotrons with gel-based media showed that root growth is higher in soil

612 than in plates (Figure 8-figure supplement 1). These data support the utility of Previous

613 work has suggested that auxin levels in *Brachypodium* roots is sub-optimal for growth²⁶.

614 Pacheco-Villalobos and colleagues suggest that, in *Brachypodium*, and contrary to what

615 happens in *Arabidopsis*, ethylene represses *YUCCA* reducing the synthesis of auxin. The

616 reduced growth that we observe in plates and the high levels of ethylene that build up in

617 sealed plates²⁷ would support this mechanism.

618 Tomato plants were transformed with *Pro35S:PPyRE8o* and *ProeDR5rev:LUC2* reporters.

619 The plants showed more rapid growth than *Arabidopsis* or *Brachypodium* and required

620 fertilizer to prevent obvious signs of stress (reduced growth, anthocyanin accumulation).

621 Root systems were imaged from 17 DAS plants. Roots showed presumptive lateral root
622 primordia marked by DR5-expression (Fig 8C-D). These results show that the GLO-Roots
623 for characterizing environmental responses that are difficult to characterize otherwise method
624 can be applied to study root systems of plants and will likely be useful for studying root
625 systems of other small to medium sized model plants and for early stages of larger crop
626 plants.

627 **Discussion**

628 **GLO-Roots enables a multi-dimensional understanding of root biology**

629 Recent studies of root systems has emphasized structural attributes as important contributors
630 of root system function. Indeed, studies examining the role of genetic variants in tolerating
631 abiotic stress have demonstrated the importance of such characteristics⁸. Roots, however,
632 are highly diverse in the biology they perform and a multi-dimensional understanding of root
633 systems, which incorporates differences in signaling, metabolism and microbial association
634 as well as structure, may provide a clearer understanding of the degree to which sub-
635 functionalization of the root system plays a role in important processes such as acclimation
636 and efficient resource acquisition.

637 We have developed tools in GLO-Roots that allow for tracking multiple aspects of soil
638 physicochemical properties and root biology simultaneously. Using GLO-Roots, we are able
639 to map in 2D coordinates soil physical properties such soil moisture together with root
640 architecture traits such as directionality, growth rates and gene expression levels. All this
641 information is aggregated in layers for each x, y coordinate. Using GLO-RIA we integrate this
642 multilayer information, leveraging our ability to simultaneously and seamlessly investigate
643 root responses to environmental stimuli such as soil moisture content. Luciferase isoforms
644 that emit light at different wavelengths allow for constitutive and regulated promoters to be
645 studied together. Introduction of luciferase reporters into microbes provides an additional
646 layer of information that provides a readout on the association between organisms and how

647 this might be affected by environmental conditions. The flexibility of the GLO-Roots system
648 may enable additional dimensionality to our understanding of root biology. Other physical
649 properties such as CO₂ or pH mapping in rhizotrons have already been enabled by using
650 planar optodes⁴¹²⁸. It may be possible to engineer LUX-based reporters in microbes that are
651 responsive to extracellular metabolites, creating microbial biosensors, and integration of such
652 tools may enable root-exudation and nutrition to be analyzed in soil. Split-Luciferase reporters
653 have been engineered that allow bi-molecular interactions to be studied. Finally, molecular
654 sensors analogous to FRET sensors, termed BRET-sensors⁴²²⁹, may allow metabolite tracking
655 dynamically through the root system. With additional innovation in the development of
656 luciferase reporters, the GLO-Roots systems will likely expand the repertoire of biological
657 processes that can be studied over an expanded range of developmental time points and
658 environmental conditions.

659 ~~Limited phosphorus availability promotes foraging in upper layers of~~
660 ~~soil~~Enhanced root growth and gravitropism may constitute an avoidance
661 mechanism used during water deficit stress

662 Phosphorus availability is one of the major limitations for plant growth and an important
663 factor influencing root architecture⁴³. P is usually more abundant in the top layers of the
664 soil where it is bound to organic matter and clay minerals. Modeling studies have suggested
665 that an increase in lateral root density and shallower root systems promote phosphorus
666 uptake since phosphorus diffusibility is limited in soil and this nutrient tends to accumulate
667 in the upper tiers of the soil column where decomposition of organic matter replenishes the
668 supply of P^{10,44}.

669 Experiments using in-vitro grown *Arabidopsis* seedlings have shown that the primary root
670 will senesce during low-P stress while lateral root growth is enhanced, however the total root
671 system area is often highly reduced. This change in root development would be expected to
672 reduce energy input into the root system, but provide little advantage in absorbing additional
673 phosphorus. Using GLO-Roots, we demonstrate that *Arabidopsis* does indeed have a robust

674 low-P response that we predict to enhance phosphorus uptake. While root system area is
675 not significantly reduced, root system width-depth ratio is increased, generating a shallower
676 root system. Differences between *in vitro* and GLO-Roots root systems may be a result of
677 the more physiologically realistic manner in which phosphorus is released to the root when
678 phosphate-buffered alumina particles are used³⁵.

679 **~~Enhanced root growth and gravitropism may constitute an avoidance mechanism~~**
680 **~~used during drought~~**

681 It has been proposed that plants with steep root systems will be better able to tap into
682 deep water resources and thus perform better under water deprivation. For example in rice,
683 the IR64 paddy cultivar shows shallow root systems in upland fields whereas Kinandang
684 Patong, an upland cultivar, is deeper rooting⁹⁸. Plants maintain a number of regulatory
685 pathways that mediate changes in physiology during WD. Enhanced growth of root systems
686 has been well characterized in field-grown plants; however this has not been recapitulated
687 in studies of gel-grown *Arabidopsis* plants. Thus, it has been unclear whether *Arabidopsis*
688 simply responds to WD differently. Our results here show that *Arabidopsis* does indeed
689 maintain a classical WD response that expands the root system and directs growth downward.
690 Interestingly, under our stress regime, we did not observe a significant decrease in the relative
691 water content of shoot tissues (Figure 11 Supplement 26-figure supplement 5), suggesting
692 that the changes in root architecture were sufficient to provide access to deep water and
693 prevent dehydration. Such changes in root growth are likely regulated through systemic and
694 local signaling that involve auxin signaling but acts independently of known pathways that
695 control moisture-directed root growth.

696 **Perspectives and Conclusions**

697 Understanding plant biology requires a sophisticated understanding of how environmental
698 stimuli affect the form and function of plants as well as an understanding of how physiological
699 context informs such responses. Environmental conditions are at least as complex as the

700 plants they affect. Plant roots are exposed to a variety of environmental signals that change
701 in time and space at very different scales that are integrated at the whole plant system. It is
702 an important challenge in biology to develop methods of growing and studying plants that
703 present such stimuli in a manner that the plant is likely to encounter in nature. After all,
704 the plants we study have evolved to survive through mechanisms that have been selected,
705 over evolutionary time, in nature. **Use of artificial conditions must be carefully considered**
706 **espeeially if adaptive mechanisms are the area of focus for the study.**

707 **The study presented here shows conclusively that root biology in soil-like media is distinct**
708 **from in vitro grown plants. These differences are not only due to media composition but**
709 **likely encompass effects from other abiotic and biotic factors as well.** It will be interesting for
710 future studies to determine how other environmental stimuli affect root growth using GLO-
711 Roots and whether these responses differ between accessions of Arabidopsis. Identification
712 of the genetic loci responsible for phenotypic variation in adult root phenotypes may identify
713 the molecular basis for adaptive variation that exists in this species and potentially identify
714 loci that are useful for breeding efforts needed for the next green revolution.

715 Materials and methods

716 Growth system

717 **Rhizotrons and growth system fabrication.** Rhizotrons are composed of two sheets of
718 1/8" abrasion resistant polycarbonate plastic (Makrolon AR (R)) cut to size using a water
719 jet (AquaJet LLC, Salem, OR), two acrylic spacers cut using a laser (Stanford Product
720 Realization Lab), two rubber U-channels cut to strips 30 cm long ([McMaster Carr part #](#)
721 [8507K33](#)) and two sheets of black 0.030" thick polypropylene sheets ([McMaster Carr part #](#)
722 [1451T21](#)) cut with a straight-edge razor blade. Rhizotron designs were drafted in Adobe
723 Illustrator (Adobe, San José, CA). The blueprints of all the parts are provided in Supplement
724 1. The top edge of each polycarbonate sheet was painted with black 270 Stiletto nail polish
725 (Revlon, New York, NY).

726 **Boxes and holders.** Rhizotrons are held vertical during plant growth in a custom rack
727 system composed of two sheets of 1/4" black acrylic plastic cut with slots for eleven rhizotrons
728 using a laser, four 3/8" PVC rods ([McMaster Carr part # 98871a041](#)) secured with PVC
729 nuts ([McMaster Carr part # 94806a031](#)) to hold the acrylic sheets horizontal. The rack is
730 placed inside a 12" x 12" x 12" black polyethylene tank ([Plastic Mart part # R121212A](#)).

731 **Rhizotron preparation** The procedure to construct a rhizotron with soil is as follows:
732 Two pieces of polycarbonate plastic are laid flat on a table with the spacers inserted. Using
733 an electric paint gun, a fine mist of water is applied to the bare polycarbonate sheets. Then,
734 using a 2 mm sieve (US Standard Sieve Series N° 10) a fine layer of PRO-MIX(r) PGX soil
735 (Premier Tech, Canada) is applied. Excess soil is discarded by gently tapping the plastic
736 against the table in a vertical position. Water is sprayed again onto the soil, then a second
737 layer of Pro-MIX is applied as before. For P deficiency experiments soil supplemented with 1
738 ml of 100 µM P-Alumina (control) and 0-P-Alumina (P deficient) was used. To prevent the
739 soil from falling out of the bottom opening, a 3 x 6 cm piece of nylon mesh is rolled into a 1
740 cm wide tube and placed at the bottom side of the rhizotron. The spacers are removed and
741 replaced by clean spacers. The two faces of the rhizotron are carefully joined together and
742 two rubber U-channels slipped on to clamp all pieces together. Assembled rhizotrons are
743 placed into the rack inside the boxes and 500 mL of water is added to the box.

744 **Plant growth** *Arabidopsis thaliana* seeds were stratified for 2 d at 4 °C in Eppendorf tubes
745 with distilled water. Seeds were suspended in 0.1 % agar and 5 to 10 were sown using a
746 transfer pipette in the rhizotron. A transparent acrylic sheet was mounted on top of the box
747 and sealed with tape to ensure high humidity conditions that enable *Arabidopsis* germination.
748 Three days after sowing, the cover was unsealed to decrease humidity and allow the seedlings
749 to acclimate to a dryer environment. From 3 days after sowing (DAS) to the time the first
750 true leaves emerged, it was critical to ensure that the top part of the rhizotron remained
751 humid for proper germination of the plants. Between three and five DAS the rhizotrons
752 were thinned leaving only the number plants required for that experiment, typically one,
753 except for experiments examining root-root interactions. Unless otherwise stated, all the

754 experiments presented here, treatments were started 10 DAS. Plants were grown under long
755 day conditions (16 h light / 8 h dark) using 20–22 °C (day/night) and 150 µE m⁻¹ s⁻¹. Two
756 types of growth environments were used for experiments. A walk-in growth chamber with
757 fluorescent lightning and a growth cabinet with white LED lights. Relative water content
758 measurements were done as previously described???

759 **qRT-PCR analysis.**

760 Seeds were surface sterilized as described before² and grown in rhizotrons, 100 cm³ pots, or
761 on two types of 1% agar (Duchefa) media containing either 1x MS nutrients (Caisson) and 1%
762 Sucrose, (termed ms media) or ¼x MS nutrients only (termed ms25 media). Both media were
763 buffered using 0.5 g/L MES and pH was adjusted to 5.7 with KOH. All plants were grown
764 together in a growth cabinet with LED lights under long day conditions (16h day/8h night).
765 Root and shoot tissue was collected separately from individual plants at the end of the day
766 (1 hour before the lights shut off) and at the end of the night (1 hour before lights came on).
767 Three biological replicates were collected for each condition. RNA was extracted using the
768 Plant RNA MiniPrepTM kit (ZYMO Research) according to manufacturer's instructions
769 with on-column DNase treatment (Qiagen). cDNA was made using the iScript Advanced
770 cDNA Synthesis for RT-qPCR kit (Bio-Rad) from 200 ng of total RNA. qRT-PCR was
771 performed using a Fluidigm BioMarkTM 96.96 Dynamic Array IFC with the EvaGreen®
772 (Bio-Rad) fluorescence probe according to the Fluidigm Advanced Development Protocol
773 number 37. For the analysis, all the reactions with no amplification (Ct = 999) were either
774 removed (if the other technical duplicate amplified) or set to the maximal Ct for that assay
775 type. The two technical replicates were then averaged and dCt values calculated using
776 AT3G07480, AT4G37830, At1g13320 and At1g13440 as reference internal controls. PCA
777 plots were generated with Devium Web⁴⁵³⁰ using log-dCt values. dCT values were calculated
778 as dCT = CT~gene interest~ - mean(CT~reference gene~). Primers used are listed in file
779 Supplement 8.

780 **Biological components**

781 **Codon optimization of luciferases.** The following luciferases that emit light at different
782 wavelengths were codon optimized for Arabidopsis (Genscript, Piscataway, NJ): LUC2: a
783 yellow improved version (Promega, Madison, WI) of the original *Photinus pyralis* (firefly)
784 LUC.

- 785 • Ppy RE8: a red variant⁴⁶³¹ of the *P. pyralis* thermostable variant Ppy RE-TS⁴⁷³².
- 786 • CBG99: a green variant (Promega, Madison, WI) from yellow click beetle (*Pyrophorus*
787 *plagiophthalmus*) luciferases.
- 788 • CBR: a red variant (Promega, Madison, WI) from yellow click beetle.

789 **Non-optimized luciferases.** We also used the following non-optimized luciferases:

- 790 • nanoLUC: a blue luciferase isolated from a deep sea shrimp⁴⁸¹².
- 791 • venusLUC2: a venus-LUC2 fusion reported to show higher luminescence output than
792 LUC2²³¹⁰.
- 793 • A transposon containing the bacterial luciferase-containing LUX operon was integrated
794 into the *Pseudomonas fluorescens* CH267³²¹⁶ genome by conjugation with *E. coli*
795 *SM10pir* containing pUT-EM7-LUX⁴⁹³³ and used to track root microbe colonization.
796 For inoculation 9 DAS plants were inoculated with 2 mL of an overnight bacterial
797 culture resuspended in 10 mM MgSO₄ and diluted to 0.01 OD.

798 **Generation of single-reporter transgenic plants.** We generated transcriptional fu-
799 sions of all luciferases to constitutive promoters to examine the activity level and emission
800 spectrum of each isoform. The *attL1-attL2* L2*-entry clones containing plant-codon opti-
801 mized coding sequence of *LUC2*, *PpyRe8*, *CBG99* and *CBR* were synthesized by Genscript.
802 A DNA fragment including the *UBQ10* promoter region and first intron was amplified from

803 Col-0 genomic DNA with primers incorporating the attB1, attB4 combination sites at the
804 5' and 3' respectively. The PCR product was then introduced into pDONRTM P4-P1R
805 (Invitrogen) through a classic Gateway BP-reaction. The resulting plasmid, the *attL1-attL2*
806 entry clones with luciferase sequences, an empty *attr2-attL3** entry clone and the destination
807 vector dpGreenmCherry² were used to construct *ProUBQ10:LUC2o*, *ProUBQ10:PpyRE8o*,
808 *ProUBQ10:CBG99o* and *ProUBQ10:CBRo* through Gateway LR reactions. The destination
809 vector *dpGreenmCherry* contains a plasma membrane-localized mCherry coding sequence
810 driven by the 35S promoter and is used as a selectable marker of transformation at the
811 mature seed stage². We used Golden Gate cloning and the destination vectors that we had
812 generated before²⁴¹¹ for the following fusions: *ProUBQ10:nanoLUC2*, *ProUBQ10:venusLUC*,
813 *ProACT2:PpyRE8o*. Briefly, the different components of each construct were PCR amplified
814 with complementary BsaI or SapI cutting sites, mixed with the destination vector in a single
815 tube, digested with either BsaI or SapI, ligated with T4 DNA ligase, then transformed
816 into E. coli Top10 cells and plated on LB antibiotic plates containing X-gal as previously
817 described²⁴¹¹. Junction sites were confirmed by sequencing. We used pSE7 (Addgene
818 ID #: pGoldenGate-SE7: 47676) as the destination vector of the *ProUBQ10:nanoLUC2*,
819 *ProUBQ10:venusLUC* constructs and pMYC2 (Addgene ID #: pGoldenGate-MCY2: 47679)
820 as the destination vector for *ProACT2:PpyRE8o*. Maps of all the vectors can be found in
821 Supplement 8. *ProUBQ10:LUC2o* was transformed into Col-0, Bay and Sha accessions, the
822 *tir1-1*⁵⁰³⁴ mutant and the *miz1*⁵¹³⁵ T-DNA insertion line (SALK_126928).

823 **Brachypodium distachyon** The Arabidopsis plant-codon optimized Luciferase gene,
824 *LUC2o*, was inserted into the monocot vector pANIC10 via Gateway cloning²⁹²⁵. *Brachy-*
825 *podium distachyon* plants were transformed using the method of Vogel and Hill⁵²³⁶.

826 **Tomato** The transcriptional fusion *ProeDR5:LUC2* was generated by cloning the
827 *ProeDR5:LUC2* DNA fragment into the pBIB expression vector via restriction sites SalI
828 and Acc65I. The eDR5 promoter is an enhanced version of DR5 containing 13 repeats
829 of the 11-nucleotide core DR5 element⁵³³⁷ and the pBIB expression vector contains an

830 NPTII resistance gene under the control of the NOS promoter for use as a selectable
831 marker during transformation. ~~This construct was transformed into the XYZ cultivar of~~
832 ~~tomato~~All tomato transformations were performed by the Ralph M. Parsons Foundation
833 Plant Transformation Facility (University of California, Davis).

834

835 **Generation of dual-reporter plants.** To generate dual-reporter plants expressing lu-
836 ciferase isoforms that emit light with divergent emission spectra we used *ProACT2:PpyRE8o*
837 as the root structural marker and ZAT12:LUC³⁴¹⁵ and DR5:LUC+³³¹⁴ lines that were
838 transformed with the *ProACT2:PpyRE8o* construct. All constructs were transformed using
839 a modified floral dip method as described in².

840 ~~Tomato~~The To make the dual color tomato plants, the *Pro35S:PpyRE8o* transcriptional
841 fusion was generated by putting the plant-codon optimized coding sequence described above
842 into the pMDC32 expression vector through a Gateway LR reaction. The pMDC32 vector
843 contains a hygromycin resistance gene under the control of the 35S promoter for use as a
844 selectable marker during transformation. This construct was transformed into the transgenic
845 *ProeDR5:LUC2* tomato line. ~~All tomato transformations were performed by the Ralph M.~~
846 ~~Parsons Foundation Plant Transformation Facility (University of California, Davis).~~

847

848 **In vivo emission spectra of plants constitutively expressing luciferase isoforms.**
849 To generate *in vivo* emission spectra of all constitutively expressed luciferases, seeds were
850 sterilized and sown on MS plates as described before². After 8 days, seedlings were treated
851 with a 100 µM luciferin solution, incubated at room temperature for 3 hours and imaged
852 using an IVIS Spectrum imaging system (Perkin Elmer, ~~bla, bla~~Waltham, MA) using 20 nm
853 band-pass emission filters at the following wavelengths (in nm: 490-510, 510-530, 530-550,
854 550-570, 570-590, 590-610, 610-630, 630-650, 650-670, 670-690, 690-710). Raw images were
855 analyzed using Fiji and *in vivo* emission spectra were constructed. The full emission spectra

856 of LUX and nanoLUC could not be constructed since the maximum of these two luciferases
857 is below the lower band pass filter that were available.

858 **Imaging system**

859 **Imaging system** We designed a custom imaging system (GLO1, Growth and Luminescence
860 Observatory 1) optimized for imaging dual-reporter luciferase expression in our custom
861 rhizotrons. The design was a joint effort with Bioimaging Solutions (San Diego, CA) who
862 also built the system and wrote the acquisition software that drives all the mechanical parts
863 of the system. The system is composed by two 2048 x 2048 PIXIS-XB cameras (Princeton
864 Instruments, Trenton, NJ) mounted on top of each other to capture two fields of view
865 encompassing approximately two 15 x 15 cm areas corresponding to the top or bottom of
866 the rhizotron. The cameras are fitted with a Carl-Zeiss macro lens. A filter wheel with space
867 for four, 76.2 mm filters is positioned in front of the cameras and controlled by a stepper
868 motor allowing for automated changing of the filter wheel position. We used two -542/50
869 and 450/70- custom cut Brightline(R) band-pass filters (Semrock, Rochester, NY). In single
870 color imaging mode, the filter wheel is operated without filters. Positioned in front of the
871 filter wheel is a removable rhizotron holder mounted on a stepper motor. This stepper motor
872 is also controlled by the GLO-1 software allowing automatic acquisition of images from both
873 sides of the rhizotron sequentially. The whole imaging system is enclosed in a light-tight
874 black box with a door that allows loading and un-loading of rhizotrons.

875 **Plant Imaging**

876 **Plant Imaging** Around 50 mL of 300 μ M D-luciferin (Biosynth, Itasca, IL) was added to
877 soil at the top of the rhizotron. In general 5 min exposures were taken per rhizotron, per
878 side, per channel. For daily imaging experiments, plants were imaged at dawn (+/- 1 hr)
879 to reduce possible effects on diurnal rhythms of keeping plants in the dark during imaging.
880 Shoot images were taken using a Nikon D3100 camera.

881 **Image Preparation**

882 **Image Preparation** Four individual images are collected: top front, bottom front, top
883 back and bottom ~~back~~^{and}. Using an automated ImageJ macro, a composite image is
884 generated as follows: 1) To correct for differences in background values between the two
885 cameras the mean background value of each image is subtracted from 200; 2) images are
886 rotated and translated to control for small misalignments between the two cameras; 3) the
887 top and bottom images of each side are merged; 4) the back image is flipped horizontally; 5)
888 the front and back images are combined using the maximum values. When dual color images
889 are acquired this operation is repeated for each channel. The final images produced are 16-bit
890 depth and 4096 x 2048 pixels. The scale of the images is 138.6 pixels per cm. Considering
891 that an Arabidopsis roots is 100 μm this results in 1.39 pixels across an Arabidopsis root.

892 **GLO-RIA imageJ plug-in**

893 **GLO-RIA imageJ plug-in** ~~The GLO-RIA plugin is divided in two parts:~~

894 ~~The first part (RootSystem) performs four different types of analysis: i) local analysis~~
895 ~~detects all root particles in the image and computes their position, length and direction;~~
896 ~~ii) the global analysis performs a root system level analysis and computes the total visible~~
897 ~~surface, convex hull, width and depth; iii) the shape analysis uses a combination of~~
898 ~~existing tools to extract relevant root architecture features. Directionality is acquired using~~
899 ~~the directionality plugin from ImageJ. After the number of direction bins (we usually use~~
900 ~~bins of 2 °) is defined by the user, a 5x5 sobel operator is used to derive the local gradient~~
901 ~~orientation. This orientation is then used to build a distribution of directions by assigning~~
902 ~~the square of the orientation into the appropriate bin. Instead of representing the total~~
903 ~~counts at each orientation a relative value is calculated by dividing the individual values at~~
904 ~~each bin by the total sum of the histogram (and multiplying by 100). Similar algorithms~~
905 ~~have been used to quantify dynamic changes in the plant cytoskeleton³⁸.~~

906 ~~The Elliptic Fourier Descriptors to perform a shape analysis on are aquired using the~~
907 ~~Fourier Shape Analysis plugin on convex hull shape of the root system convex hull iv) the~~

908 directionality analysis computes the mean direction of root particles in a. Elliptic Fourier
909 Descriptors have been used in numerous studies to analyse variations in shapes, notably in
910 leaves (e.g.???) The shape analysis is inspired by RootScape???. Due to the absence of fixed,
911 recognisable structures in root system (either on the full image or by user-defined sections
912 of the image). These four analysis are fully automated by default, but can be manually
913 adjusted if needed.

914 The second part of GLO-RIA (RootReporter) was specifically designed for the analysis of
915 dual reporter images (gene reporter and a root structural reporter) that are required for
916 the position of true landmarks), pseudo-landmarks are automatically extracted from the
917 root systems. Shortly, the plugin works as follow: i) detection of the gene reporters and
918 the structure reporters in their respective images; ii) if needed, a manual correction can
919 be performed to correct the automated detection; iii) gene reporters are linked with the
920 structure reporters, based on their proximity; iv) gene reporter intensity (either absolute or
921 normalized using the structural reporter) is computed; v) all data are exported and saved to
922 an RSML datafile⁵⁴. Gene and structure reporters can be followed across different time and
923 space points. image is divided vertically at equidistant positions (with the number defined by
924 the user) and for each of the image stripes, the minimum and maximum x coordinates are
925 computed. The shape analysis is therefore able to discriminate root system with different
926 vertical root distributions or global root system orientation (e.g. chemotropism). The code
927 source for the plugin, manual and sample images can be found in the github repository of
928 the project.

929 Statistical analysis was performed in R⁵⁵³⁹. The tidyR⁵⁶⁴⁰, dplyr⁵⁶⁴⁰, gridExtra⁵⁷⁴¹ and
930 shapes⁴², geomorph⁴³, ggplot2⁵⁸⁴⁴ and cowplot^{???} packages were used for data preparation,
931 analysis and plotting. Final figure preparation was done in Inkscape.

932 Data availability

933 **Data availability** All the scripts and original data used to analyze and pro-
934 duce the images can be accessed in the Github repository of the project: [35](https://github.com/rr-</p></div><div data-bbox=)

935 lab/[gleGLO-Roots](#). Raw files of all the images used in the paper ~~is~~are availabe in Dryad.

936 **Acknowledgements**

937 Work in the lab of JRD was funded by the Carnegie Institution for Science Endowment and
938 grants from the National Science Foundation (MCB-115795) and Department of Energy,
939 Biological and Environmental Research program (DE-SC0008769). RRA was supported by a
940 Carnegie Postdoc Fellowship and currently by Conacyt Ciencia Básica Joven Investigador
941 grant number (CB-2014-01-238101). GL was supported by the Belgian Fonds de la Recherche
942 Scientifique. JM was funded by the National Science Foundation (IOS-0820854). CH is
943 funded by MGH Toteston & Fund for Medical Discovery Fellowship grant 2014A051303
944 and NIH R37 grant GM48707 and NSF grant MCB-0519898 awarded to Frederick Ausubel,
945 and previously by the Gordon and Betty Moore Foundation through Grant GBMF 2550.01
946 from the Life Sciences Research Foundation. JV was funded by the Office of Biological
947 and Environmental Research, Office of Science, US Department of Energy, interagency
948 agreements DE-SC0001526 and DE-AI02-07ER64452. We thank Robert Mittler and Philip
949 Benfey for providing seeds of ZAT12:LUC and DR5:LUC+ respectively. We also thank
950 Neil Robbins [and members of the Dinneny lab](#) for critical review of the manuscript ~~an~~and
951 suggestions during the development of the project. We greatly appreciate Tim Doyle [at the](#)
952 [Stanford Small Animal Imaging Facility for providing](#) ´s advice [in using](#) and help with ~~mul~~
953 [luciferase-based imaging approaches.](#)

954 **Competing interests**

955 We do not have any competing interests that we are aware of.

956 **Tables**

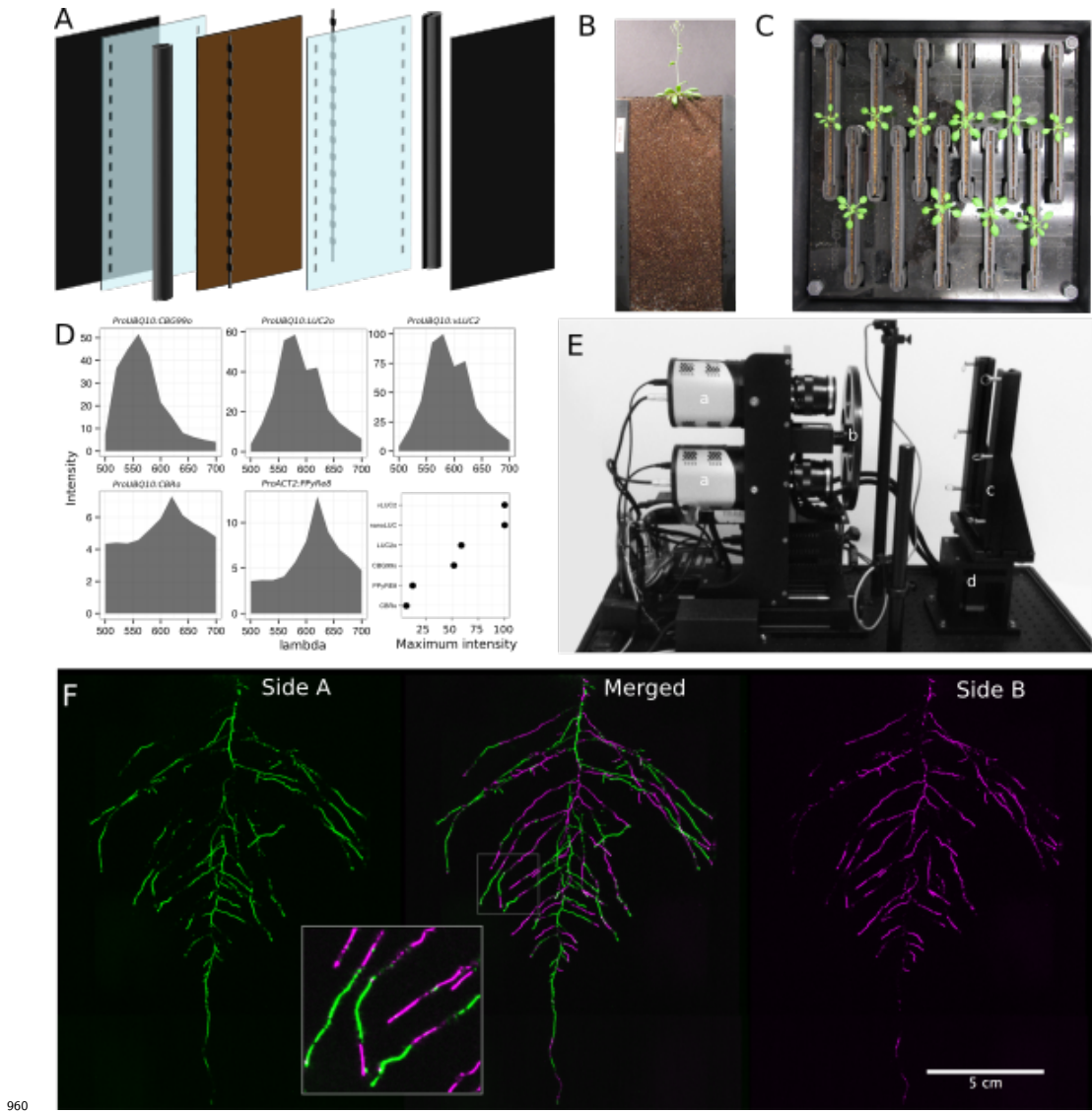
957 **Table 1:** Luciferases used in this study.

Luciferase	Origin	maximum wavelength	Substrate
Ppy RE8	firefly	618	D-luciferin
CBGRed	click beetle	615	D-luciferin
venus-LUC2	FP + firefly	580	D-luciferin
LUC(+)	firefly	578	D-luciferin
CBG99	click beetle	537	D-luciferin
lux operon	A. fischeri	490	biosynthesis pathway encoded within operon
nanoLUC	Deep sea shrimp	470	furimazine

958 **Table 2:** list of root system features extracted using GLO-RIA.

variable	unit
projected area	cm ²
number of visible roots	-
depth	cm
width	cm
convex hull area	cm ²
width	cm
feret	cm
feret angle	°
circularity	-
roundness	-
solidity	-
center of mass	cm
Directionality	°
Euclidean Fourier Descriptors	-
Pseudo landmarks	-

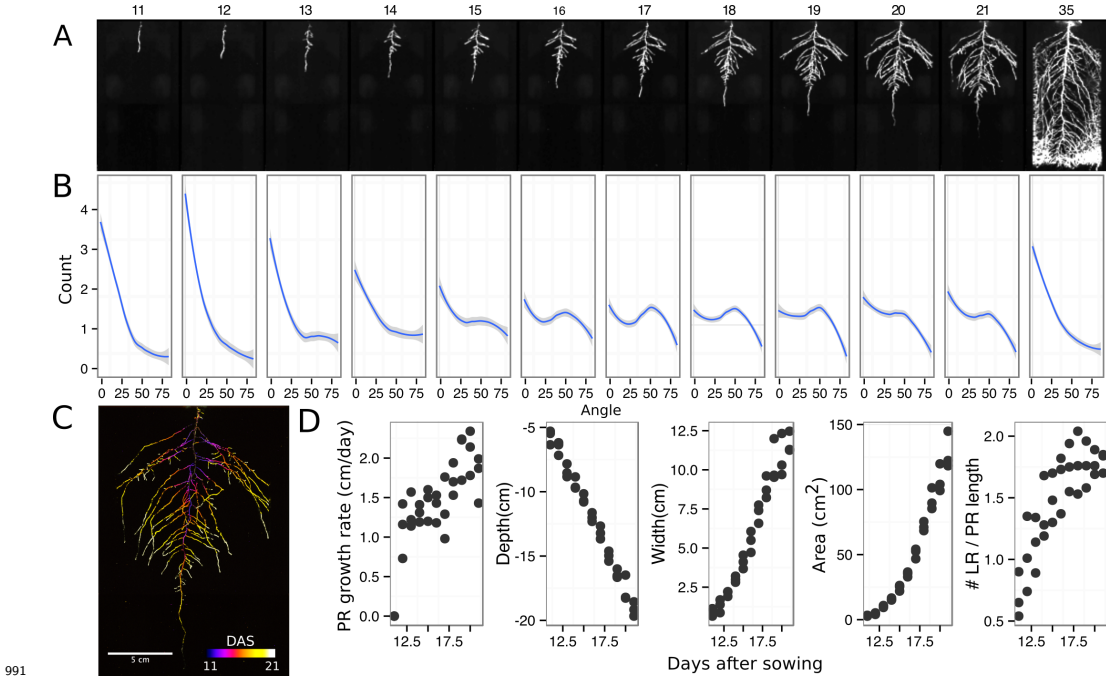
959 **Figures**



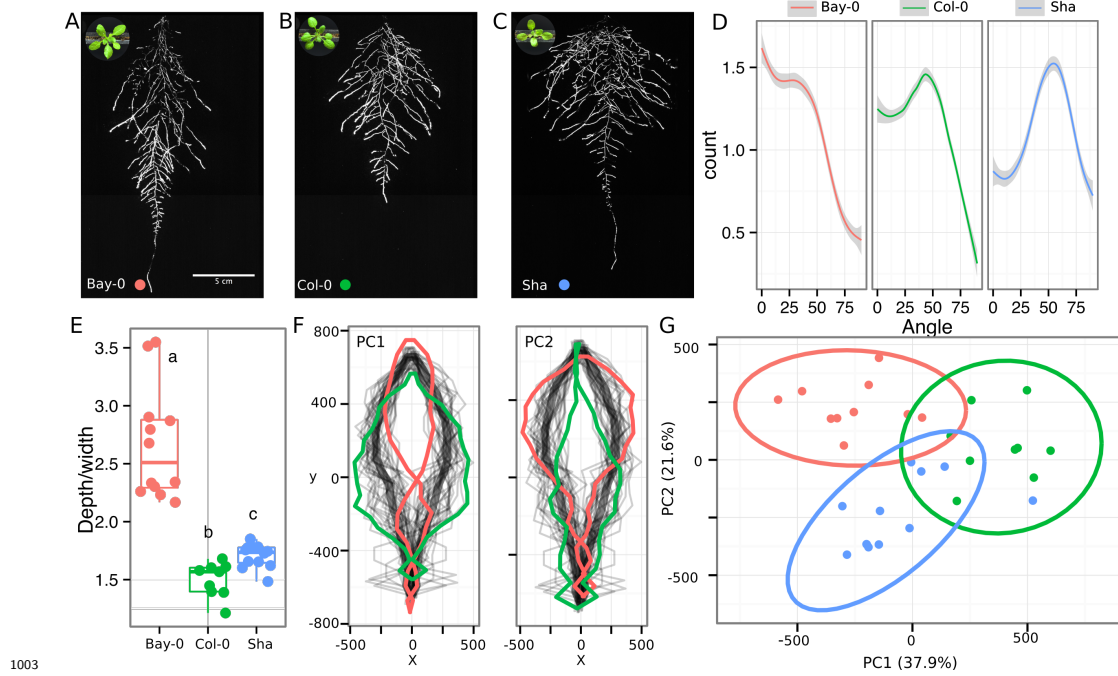
960
961 **Figure 41. GLO-Roots growth and imaging systems** -A) 3D representation of the
962 different physical components of the rhizotron: plastic covers, polycarbonate sheets, spacers
963 and rubber U-channels. Blueprints are provided in Supplementary material 1. In brown, soil
964 layer. B) Thirty five ~~days old~~ day-old plant in rhizotron with black covers removed. C) Top
965 view of holding box with eleven rhizotrons. D) Principal Components Analysis (PCA) score
966 plot of a set of 77 genes analyzed by qPCR from root samples of plants grown in MS plates,

967 pots, and rhizotrons. After 15 DAS three plants were collected at the end of the day (D)
968 and three were collected at the end of the night (N). (ms = plant grown in full ms, ms²⁵
969 = plants grown in 25% of full ms) E) Heat map of genes that were significantly different
970 between rhizotrons and media in either day or night or both. We used p-value < 0.00065
971 threshold based on Bonferroni adjustment for multiple testing. F) Lateral root number and
972 G) primary root length of 18 DAS plants grown in 30 cm tall cylinders, pots and rhizotrons,
973 all with a volume of 100 cm³ (n = 6-12 plants). H) Leaf area and I) primary root length
974 of plants of the same age (15 DAS) as the ones used for the qPCR experiment (n = 6-7).
975 ANOVA analysis with p < 0.01 was used to test significant differences between the different
976 parameters.

977 **Figure 2:** A) In vivo emission spectra of different luciferases used in this study. Transgenic
978 homozygous lines expressing the indicated transgenes were grown on agar media for 8 days.
979 Luciferin (300 µM) was sprayed on the seedlings and plates were kept in the dark and then
980 imaged for 2 s at wavelengths ranging from 500 to 700 nm. Five intensity values were taken
981 from different parts of the roots of different seedlings and averaged. Relative maximum
982 intensity values are indicated in the lower right graph. B) GLO 1 imaging system. The
983 system is composed by two back illuminated CCD cameras (a) cooled down to -55 °C. A
984 filter wheel (b) allows for spectral separation of the different luciferases. On the right, a
985 rhizotron holder (c) is used to position the rhizotrons in front of the cameras. A stepper
986 motor (d) rotates the rhizotron 180° to image both sides. C) A 21 DAS plant expressing
987 *ProUBQ10:LUC2o* was imaged on each of two sides of the rhizotron; luminescence signal is
988 colorized in green or magenta to indicate side. In the middle of the panel, a combined image
989 of the two sides is shown. The inset shows a magnified part of the root system. FW: fresh
990 weight, PR: Primary root.



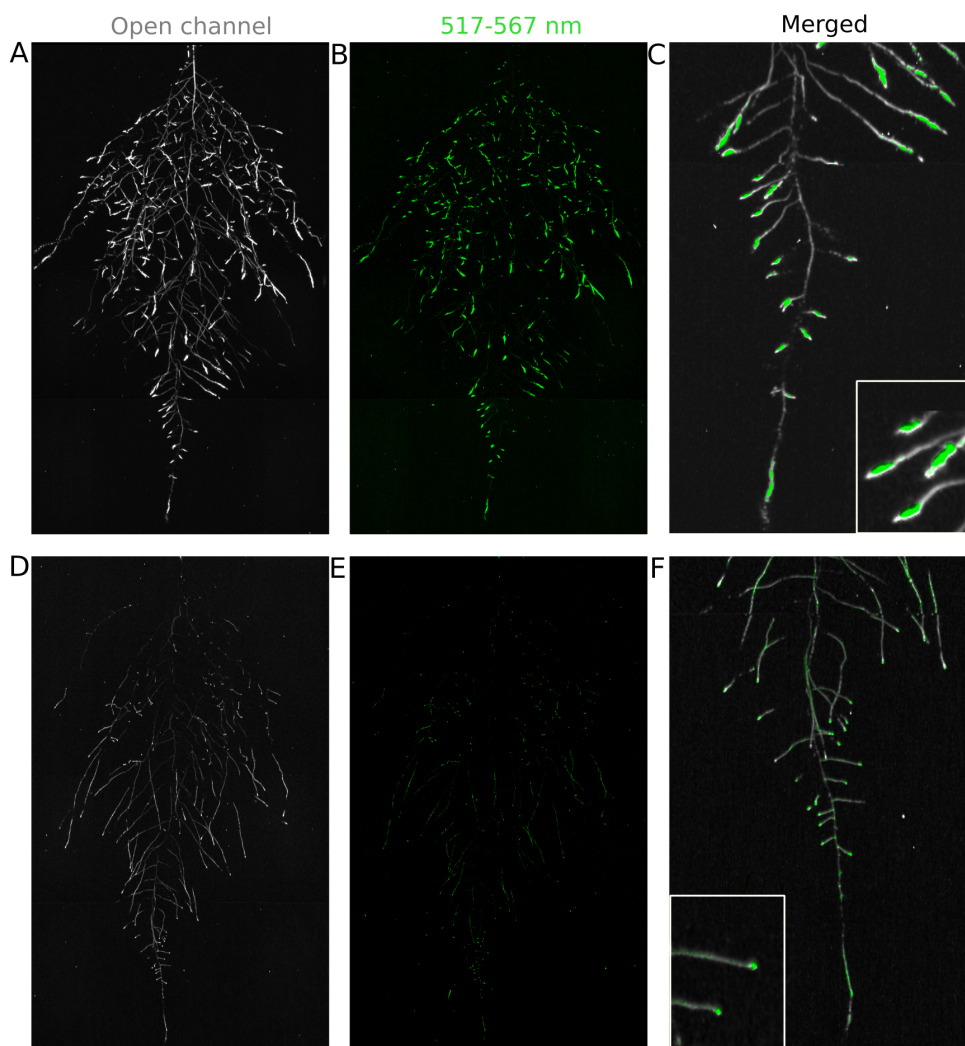
992 **Figure 32.** Time-lapse imaging of root systems and quantification using
993 GLO-RIA. A) Typical daily time-lapse image series from 11 to 21–35 DAS of a
994 *ProUBQ10:LUC2o* Col-0 plant. B) Color-coded projection of root growth using the images
995 in panel A. C) Directionality of the root system of plants in panel A calculated using the
996 directionality plugin implemented in GLO-RIA. C) Color coded projection of root growth
997 using the images in panel A. D) Primary root growth rate, depth, width, root system area
998 are automatically calculated from the convex hull, which is semi-automatically determined
999 with GLO-RIA. Lateral root number and number of lateral roots divided by the primary
1000 root length were quantified manually. A Local Polynomial Regression Fitting with 95%
1001 confidence interval (grey) was used to represent the directionality distribution curve. (0° is
1002 the direction of the gravity vector).



1004 **Figure 43. Variation in root architecture between accessions of Arabidopsis.**
1005 ~~1005~~ Representative root and shoot images of A) Bay-0, B) Col-0 and C) Sha accessions
1006 ~~transformed with ProUBQ10:LUC2o and imaged after 22 DAS transformed with~~
1007 ~~ProUBQ10:LUC2oDAS. D) Directionality of the root systems, E) root area, F) depth/width~~
1008 ~~ratio G) vertical center of mass of Bay-0, Col-0 and Sha accessions. ANOVA analysis with~~
1009 ~~p < 0.01 was used to test significant differences between the different parameters (n = 3).~~
1010 ~~F) Pseudo-landmarks describing shape variation in root system architecture. Eigenvalues~~
1011 ~~derived from the analysis of 9-12 plants per accession is shown. The first two~~
1012 ~~Principal Components explaining 38% (PC1) and 22% (PC2) of the shape variation are~~
1013 ~~plotted. PC1 captures homogeneity of root system width along the vertical axis and PC2~~
1014 ~~a combination of depth and width in top parts of the root system. Red and green lines~~
1015 ~~indicate -3SD and +3SD (Standard Deviations), respectively G) PC separation of the~~
1016 ~~different ecotypes using the PCs described in (F). A Local Polynomial Regression Fitting~~
1017 ~~with 95% confidence interval (grey) was used to represent the directionality distribution~~
1018 ~~curve. (0° is the direction of the gravity vector).~~

1019 **Figure 5:** Roots of *Brachypodium distachyon* transformed with *ProZmUB1:LUC2o* and

1020 imaged at 15 (A) and 24 (B) DAS grown in control conditions. B) Depth of the primary
 1021 root of *Brachypodium* plants grown in rhizotrons or on gel-based media. Wilcoxon test
 1022 analysis with $p < 0.01$ was used to test significant differences between the different accession
 1023 ($n = 8-11$). C) 14 DAS tomato plant transformed with *ProeDR5rev:LUC2o* (magenta) and
 1024 *Pro35S:PPyRE8o* (grey). D) Zoomed inset of root in panel C showing increased expression
 1025 of *ProeDR5rev:LUC2o* reporter in early-stage lateral roots. (9-12 plants).

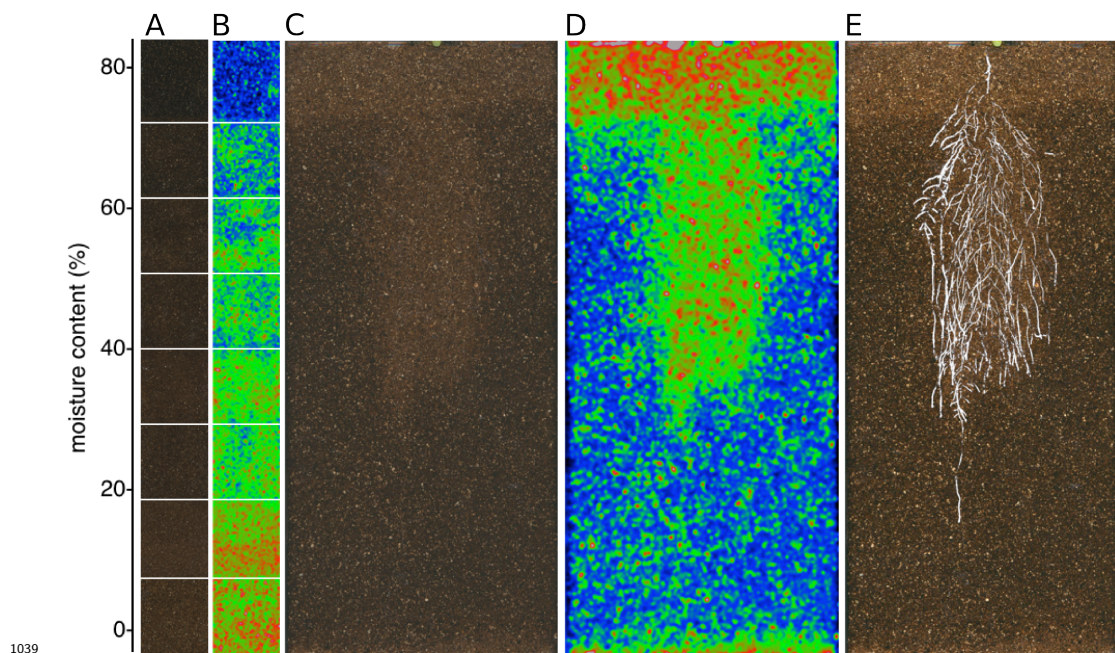


1026
 1027 **Figure 6:** A) Triple color picture showing a 22 DAS *ProUBQ10:LUC2o* plant (magenta)
 1028 grown in the same rhizotron with *ProACT2:PPyRE8o* plants (grey). Plants were inoculated
 1029 with *Pseudomonas fluorescens* CH267 (green). Magnified portion of root systems colonized

1030 by *Pseudomonas fluorescens* showing *P. fluorescences* (B) only or all three reporters
1031 together (C).

1032 **Figure 74. Dual-color reporter visualization of structure and gene expression.**

1033 → Images of whole root systems (A, E) or magnified portion of roots (B, D, C, F) at
1034 22 DAS expressing *ProDR5rev:LUC+* (magenta green, A, B) or *ProZAT12:LUC* signal
1035 (magenta, C, D green, D, E) with skeletonized representation of root roots generated using
1036 the *ProACT2:PpyRE8o* reporter expression (in grey) → E Time series showing root growth
1037 and *ProZAT12:LUC* expression after salt addition to the right side of the root system. F)
1038 Correlation of root growth and *ProZAT12:LUC* expression intensity.



1040

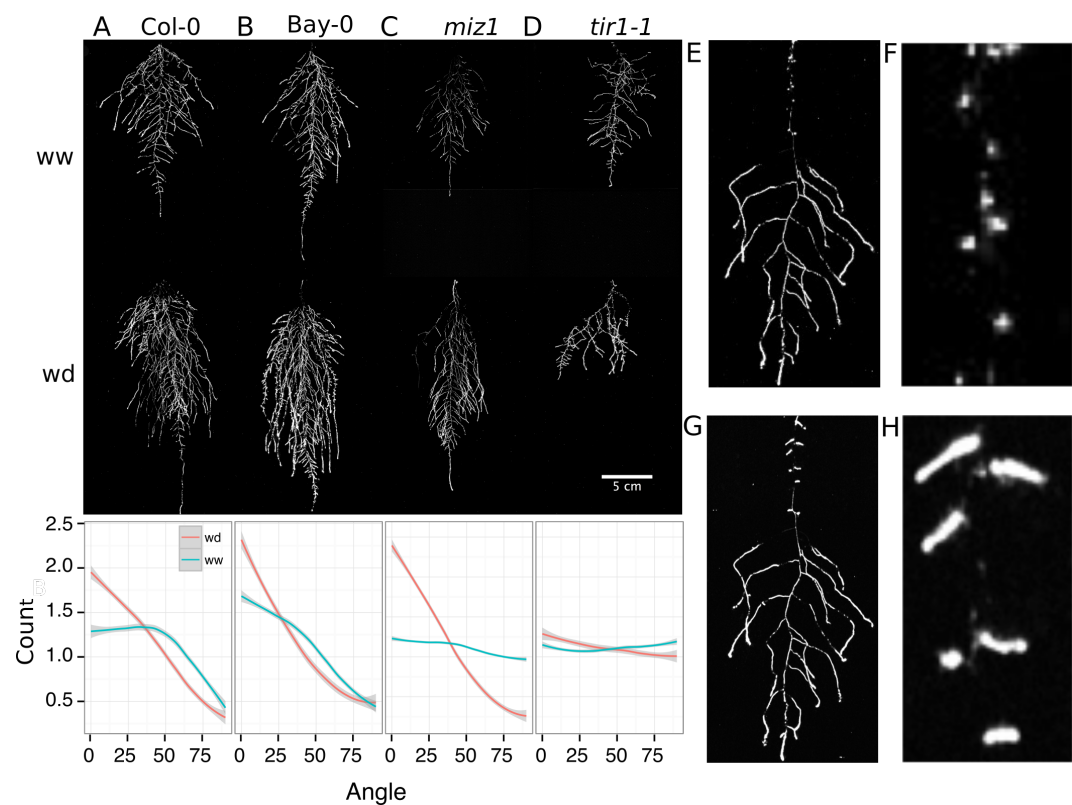
1041 **Figure 9.** A) Col-0 root systems shielded (top) or light exposed (bottom). After 9 DAS the
1042 top third of the rhizotron was exposed to light (indicated on the side with a light grey bar)
1043 and plants were imaged at 20 DAS. B) Directionality analysis of root systems shielded (red)
1044 or exposed (green) to light for Col-0 (top panel) or phot1/2 double mutant (bottom panel).
1045 Between 4 5. Soil moisture and 6 plants were analyzed per treatment. ANOVA analysis at
1046 p < 0.01 was used to compare depth/width ratios in P treatments. Kolmogorov-Smirnov

1047 test at $p < 0.001$ was used to compare directionality distributions between the different
1048 treatments. A Local Polynomial Regression Fitting with 95% confidence interval (grey)
1049 was used to represent the directionality distribution curve. (0° is the direction of the gravity
1050 vector).

1051 **Figure 10:** Soil moisture mapping in rhizotrons. A) Composite image strip root
1052 architecture mapping in rhizotrons. **Figure 8.** Shoot and root systems of
1053 *ProUBQ10:LUC2e* Col-0 plants growing in soil supplemented with 1ml of
1054 100 μ M P-Alumina (left) and 0 P-Alumina (right) 22 (A) or 27 (B) DAS.
1055 C) Root depth/width ratio of 22 (top) and 27 (bottom) DAS plants. D)
1056 Scatter-plot showing relationship between root and shoot system area at 22
1057 (top) and 27 (bottom) DAS. E) Root directionality distribution in plants 22
1058 (top) and 27 (bottom) DAS. Anova analysis at $p < 0.01$ was used to compare
1059 depth/width ratios in P treatments. Kolmogorov-Smirnov test at $p < 0.001$ was
1060 used to compare directionality distributions between the different treatments.
1061 A Local Polynomial Regression Fitting with 95% confidence interval (grey) was
1062 used to represent the directionality distribution curve. (0° is the direction of
1063 the gravity vector).

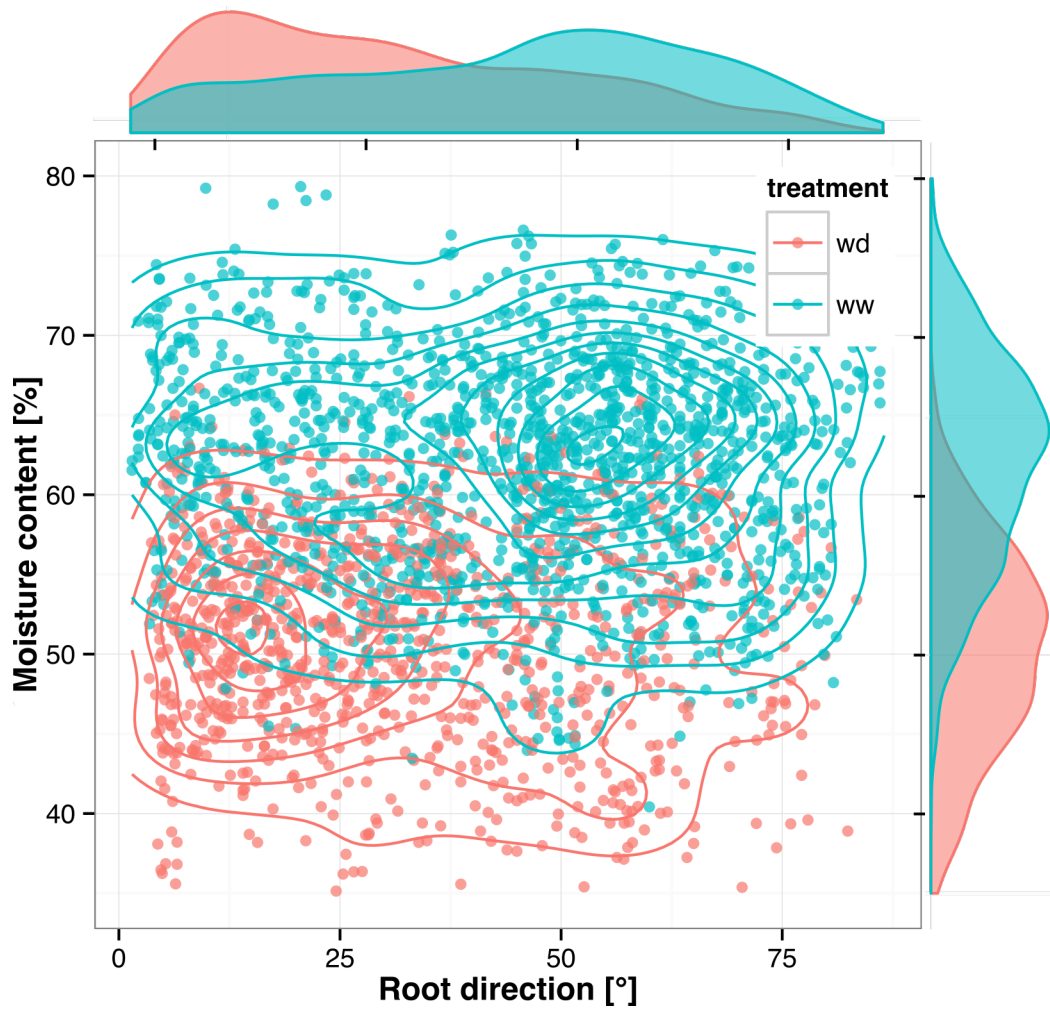
1064 **Figure 9.** A) Col-0 root systems shielded (top) or light exposed (bottom). After
1065 9 DAS the top third of the rhizotron was exposed to light (indicated on the
1066 side with a light grey bar) and plants were imaged at 20 DAS. B) Directionality
1067 analysis of root systems shielded (red) or exposed (green) to light for Col-0 (top
1068 panel) or phot1/2 double mutant (bottom panel). Between 4 μ mole
1069 and 6 plants were analyzed per treatment. ANOVA analysis at $p < 0.01$ was
1070 used to compare depth/width ratios in P treatments. Kolmogorov-Smirnov
1071 test at $p < 0.001$ was used to compare directionality distributions between
1072 the different treatments. A Local Polynomial Regression Fitting with 95%
1073 confidence interval (grey) was used to represent the directionality distribution
1074 curve. (0° is the direction of the gravity vector).

1075 **Figure 10: Soil moisture mapping in rhizotrons.** A) Composite image strip
 1076 root architecture mapping in rhizotrons. A) Composite image showing regions
 1077 of soil made from rhizotrons prepared with different soil-moisture levels. B)
 1078 Differences in grey-scale intensity values were enhanced using a 16-color Look
 1079 Up Table (LUT). Brightfield image of soil in rhizotron (C) and converted using
 1080 16-color LUT to enhance visualization of distribution of moisture (D) . E) Root
 1081 system of a Bay-0 22 DAS and subjected to water deprivation since 13 DAS.
 1082 Root system visualized using luminescence and overlaid on brightfield image of
 1083 soil in (C).



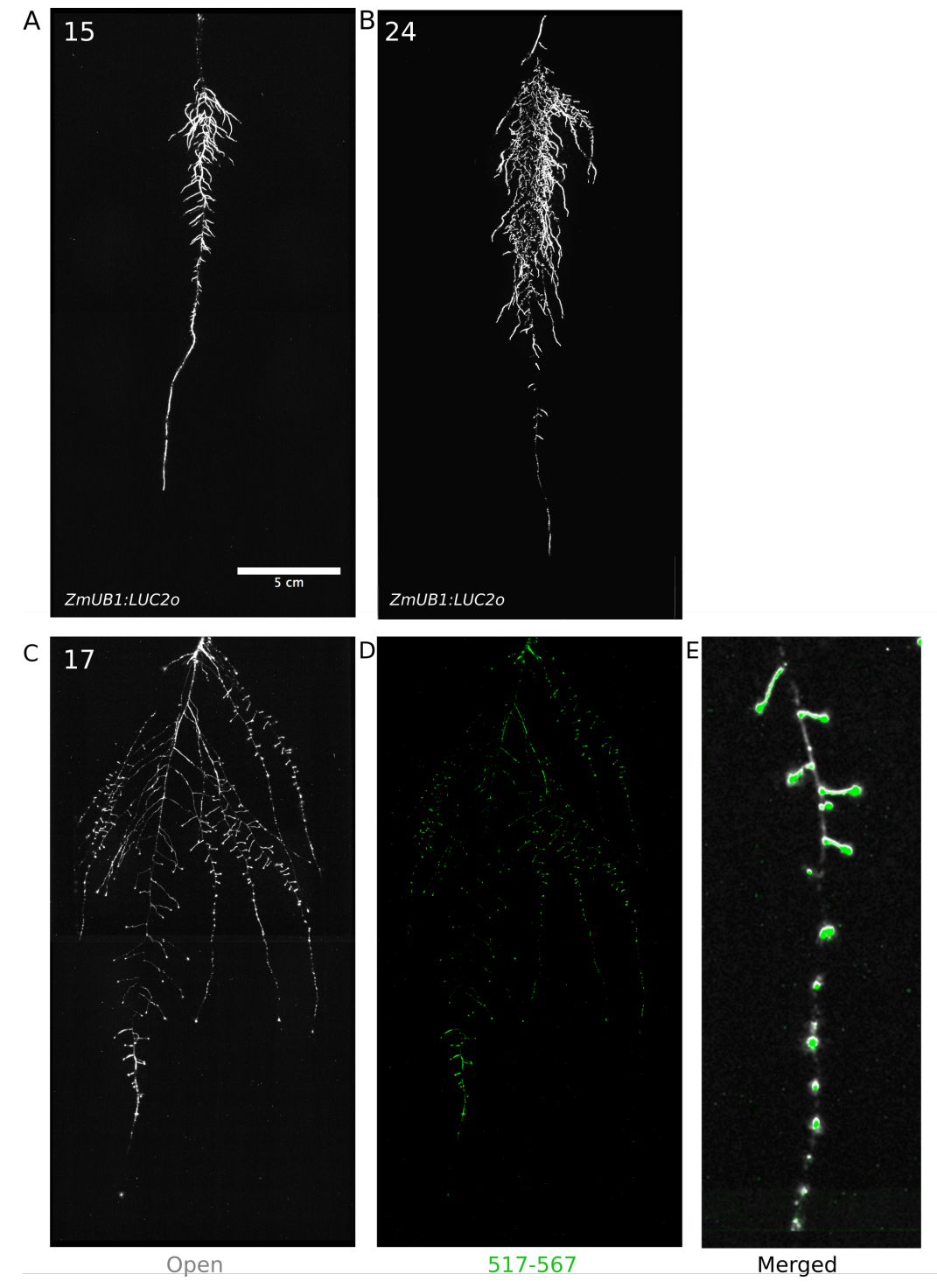
1084
 1085 **Figure 116. Study of effect of water deficit on root system architecture.** ♦
 1086 A-D) Root systems 22 DAS and exposed to water deficit 13 DAS onwards.
 1087 Sample images of well watered (left panels) and water deficit (right panels)
 1088 root systems started treated from 13 DAS and directionality (line graphs
 1089 to left of images) for (A) Col-0 (B) Bay-0 (C) *miz1* mutant and (D) *tir1-1*

1090 . E) Root system of a 22 DAS plant exposed to water deprivation from 9
 1091 DAS onwards with magnified view of lateral root primordia (F). G) The same
 1092 root as in (E) 24 hours after rewatering and magnified view of lateral root
 1093 primordia (H). Kolmogorov-Smirnov test at $p < 0.001$ was used to compare
 1094 directionality distributions between the different treatments and genotypes. A
 1095 Local Polynomial Regression Fitting with 95% confidence interval (grey) was
 1096 used to represent the directionality distribution curve. (0° is the direction of
 1097 the gravity vector).



1098
 1099 **Figure 127. Relationship between local soil moisture content and root growth**
 1100 ~~direction. :- Relationship between local soil moisture content and root growth~~

1101 direction. Data quantified from the time lapse ~~shown in series shown in Video~~
1102 2. Density plots shown at periphery of graph for root direction (x-axis) and soil
1103 moisture (y-axis). (0° is the direction of the gravity vector).~~— Data represents~~
1104 ~~2535 root tips measured in a series encompassing 10 time points.~~



1105 **Figure 8: Roots of *Brachypodium distachyon* transformed with *ProZmUB1:LUC2o***

1106

1107 and imaged at 15 (A) and 24 (B) DAS grown in control conditions. C) Open
1108 channel of 17 DAS tomato plant transformed with *ProeDR5rev:LUC2o* and
1109 *Pro35S:PPyRE8o* D) Green channel showing only *ProeDR5rev:LUC2o* E)
1110 Amplification of the open and green channel showing increased expression of
1111 *ProeDR5rev:LUC2o* reporter in early-stage lateral roots.

1112 Videos

1113 **Video 1** Time lapse from 11 to 21 DAS of a Col-0 plant expressing
1114 *ProUBQ10:LUC2o* grown in control conditions

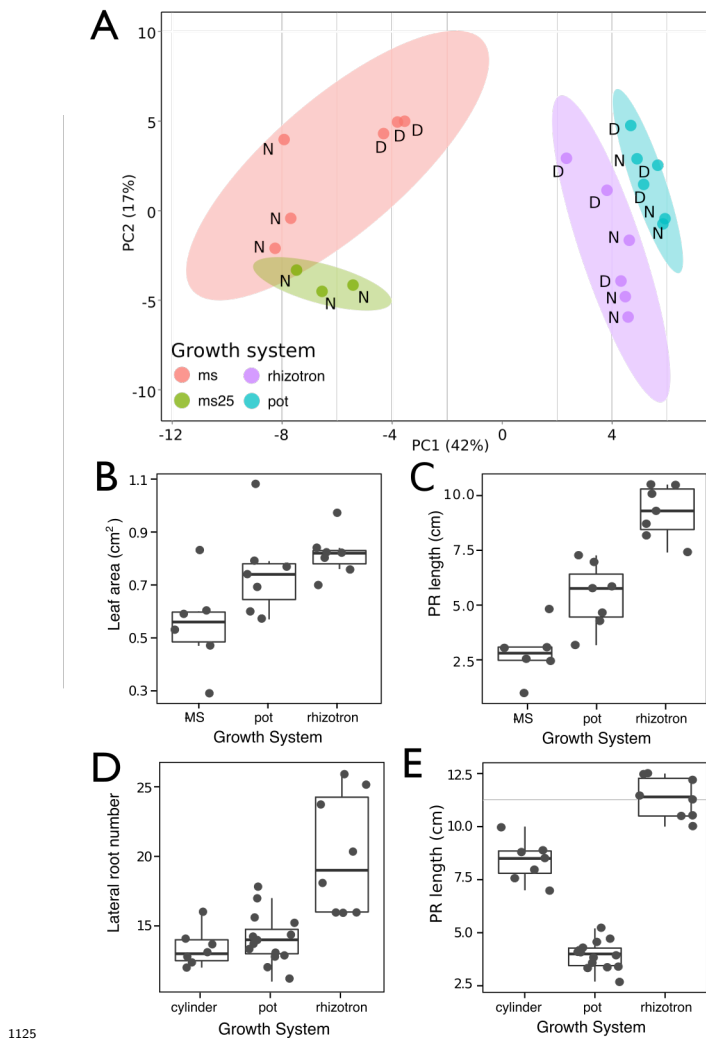
1115 ~~24 h time lapse a Col-0 plant expressing *ProACT2:PpyRE8* (gray) and~~
1116 ~~ZAT12:LUC (magenta) after addition of a 1 M solution of NaCl on the right~~
1117 ~~side of the plant.~~

1118 **Video 2** Time lapse from 16 to 24 DAS of Col-0 plants expressing
1119 *ProUBQ10:LUC2o* growing in water deficient ~~conditions~~ (left) and con-
1120 trol (right) conditions. Plants were sown under control conditions and water
1121 deficit treatment started 11 DAS. Images were taken every day.

1122

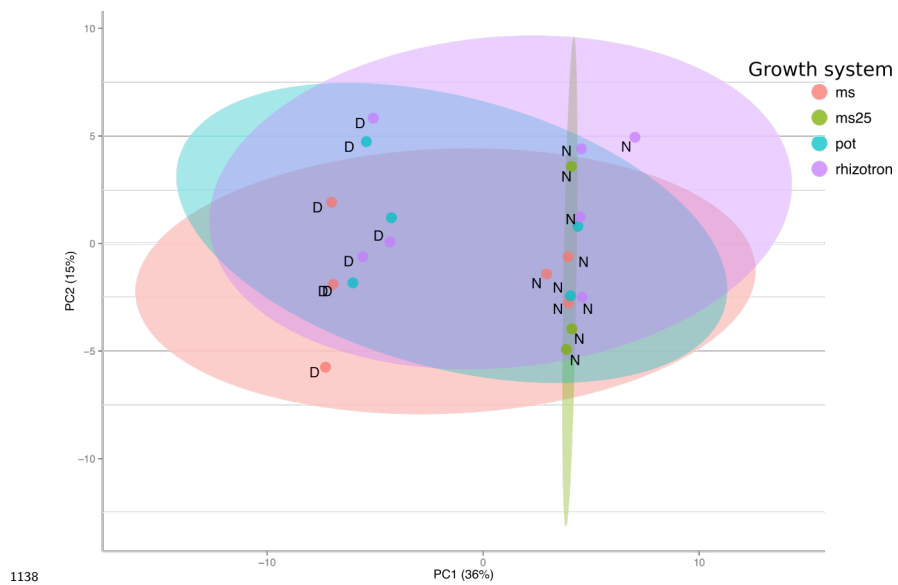
1123 **Supplementary Material**

1124 **Supplementary figures**

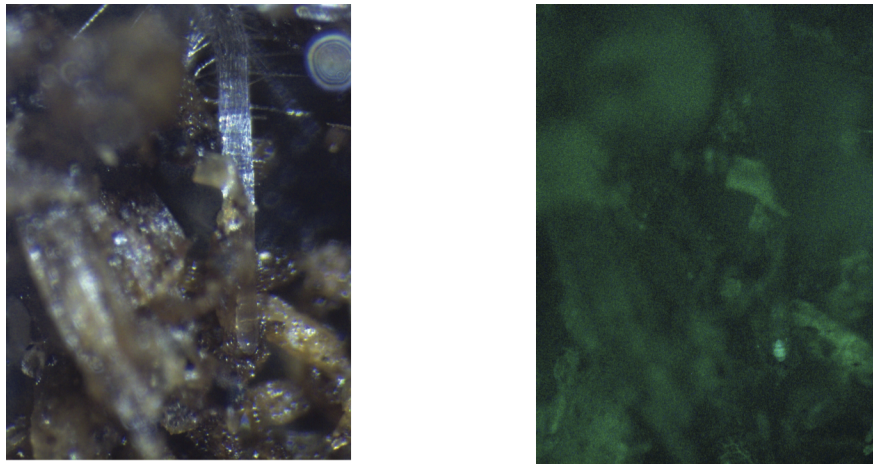


1125
1126 **Figure 1-Supplement 1PCAplot 1-figure supplement 1. Effect of different growth**
1127 **systems on plant biology. A) Principal Components Analysis (PCA) score plot**
1128 **of a set of 76 genes analyzed by qPCR from root samples of plants grown in**
1129 **MS plates, pots, and rhizotrons. After 15 DAS three plants were collected at**
1130 **the end of the day (D) and three were collected at the end of the night (N).**
1131 **(ms = plant grown in full ms and 1% sucrose, ms25 = plants grown in 25% of**

1132 full ms) B) Lateral root number and G) primary root length of 18 DAS plants
 1133 grown in 30 cm tall cylinders, pots and rhizotrons, all with a volume of 100
 1134 cm³ (n = 6-12 plants). D) Leaf area and E) primary root length of plants of
 1135 the same age (15 DAS) as the ones used for the qPCR experiment (n= 6-7).
 1136 ANOVA analysis with p < 0.01 was used to test significant differences between
 1137 the different parameters.



1138
 1139 *Figure 1-figure supplement 2. PCA plot of shoots of the same samples used
 1140 analyzed in Figure 1. See Figure 1 for more details regarding experimental
 1141 conditions used.



Brightfield

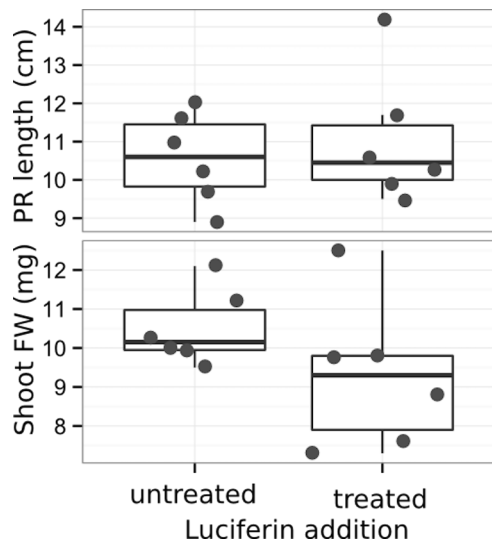
1142

GFP

1143

Figure 2 ~~Supplement 11-figure supplement 3~~ Image of an *Arabidopsis* root in soil imaged with white light (brightfield) or epifluorescence.

1144



1145

Figure 1 ~~figure supplement 4~~ Effect of luciferin addition on ~~the~~ primary root length and shoot size of 14 DAS seedlings that were either continuously exposed to 300 μ M luciferin from 9 DAS after sowing or not.

1146

Figure 6 ~~Supplement 1-figure supplement data 1~~ Dual-color images of 22 DAS plants growing in the same rhizotron and expressing different luciferases.: Two

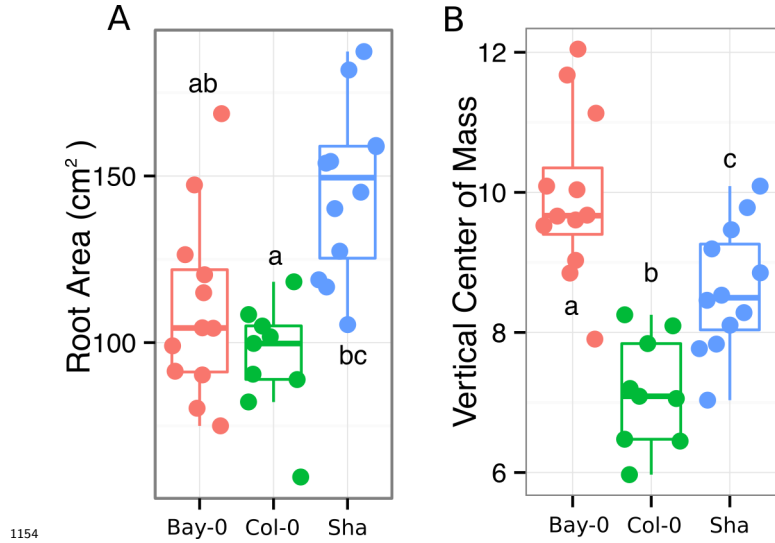
1147

1148

1149

1150

1151 way ANOVA P-values comparing plants grown in MS media vs. plants grown in
 1152 soil (pots or rhizotrons) and plants collected at day or night. We used p-value
 1153 < 0.000065 threshold based on Bonferroni adjustment for multiple testing.



1154
 1155 **Figure 3-figure supplement 1** A) root area, B) vertical center of mass of Bay-0,
 1156 Col-0 and Sha accessions.

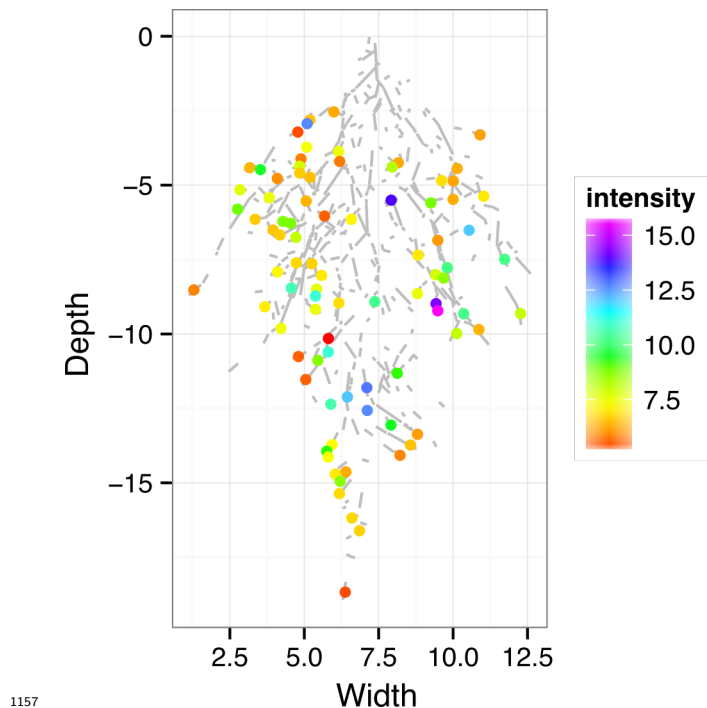
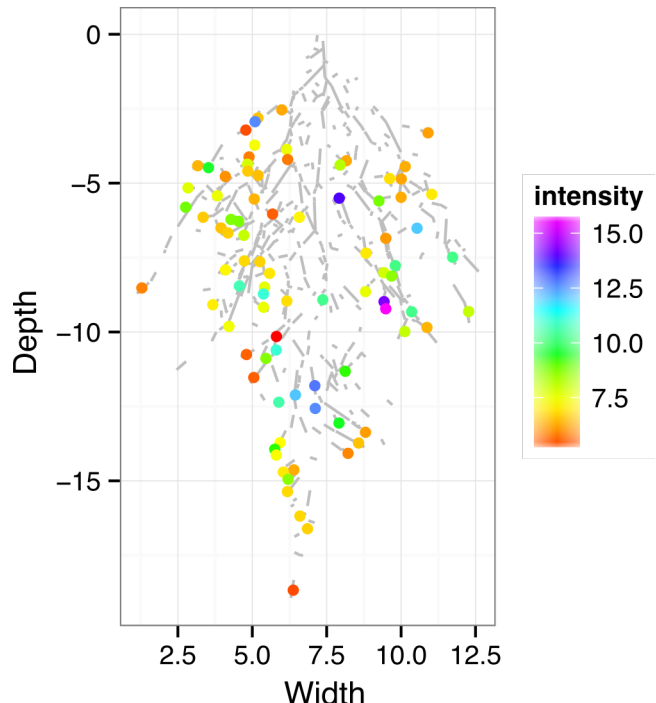
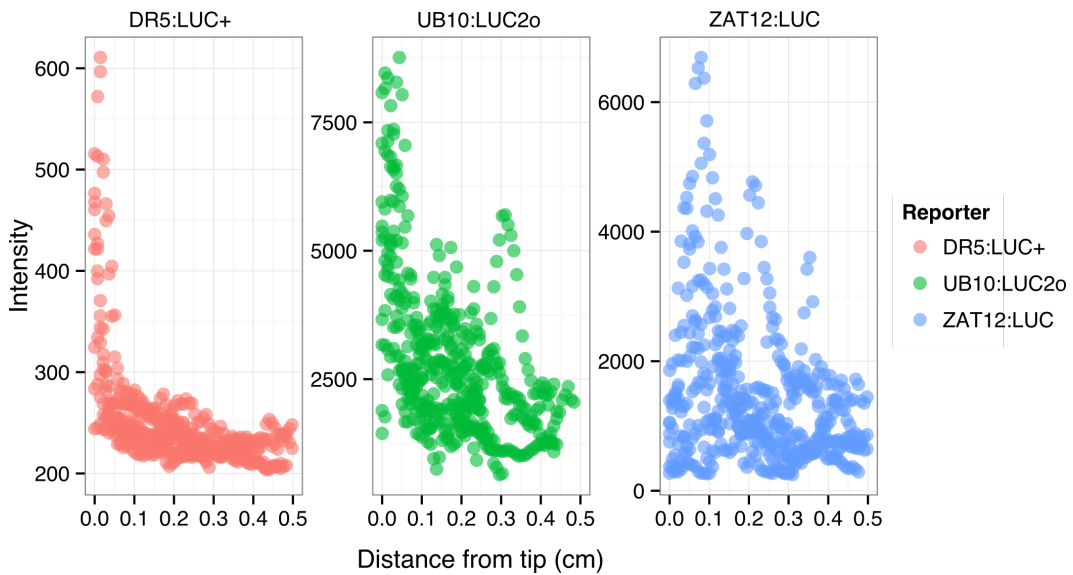


Figure 4-figure supplement 1:

1158 ZAT12:LUC intensity and root segments automatically identified values along the
1159 root tip. Data was manually obtained by obtaining the intensity profile of the
1160 first 0.5 cm from the root tip of individual lateral roots. Ten lateral roots for
1161 each reporter were measured.

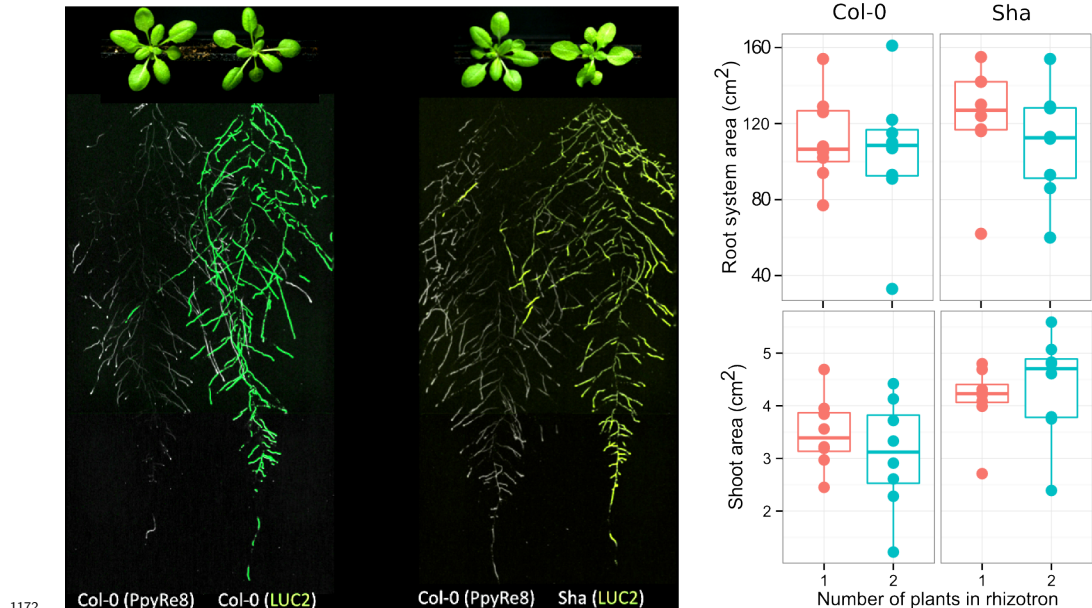


1162 Figure 4-figure supplement 2:
1163 DR5:LUC+, UBQ10:LUC2o and ZAT12:LUC intensity values along the root
1164 tip. Data was manually obtained by obtaining the intensity profile of the first
1165 0.5 cm from the root tip of individual lateral roots. Ten lateral roots for each
1166 reporter were measured.



1167

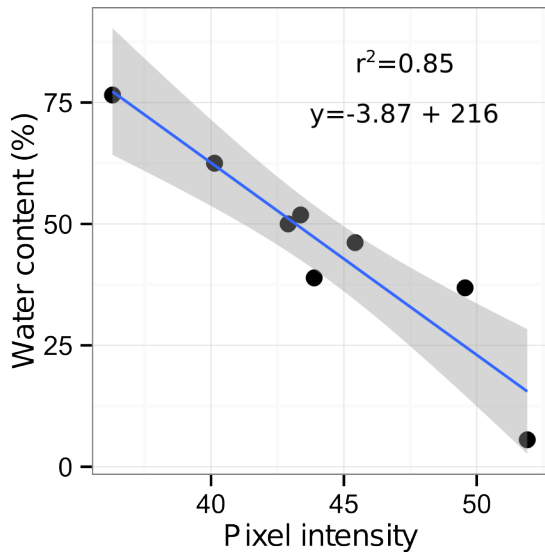
1168 **Figure 4-figure supplement 3. Images of plants at 22 DAS growing in the**
 1169 **same rhizotron and expressing different luciferases. A)** Two Col-0 plants ex-
 1170 **pressing *ProUBQ10:LUC2o* and *ProACT2:PPyRE8o* B)** Col-0 plant expressing
 1171 ***ProACT2:PPyRE8o* and Sha plant expressing *ProUBQ10:LUC2o*.**



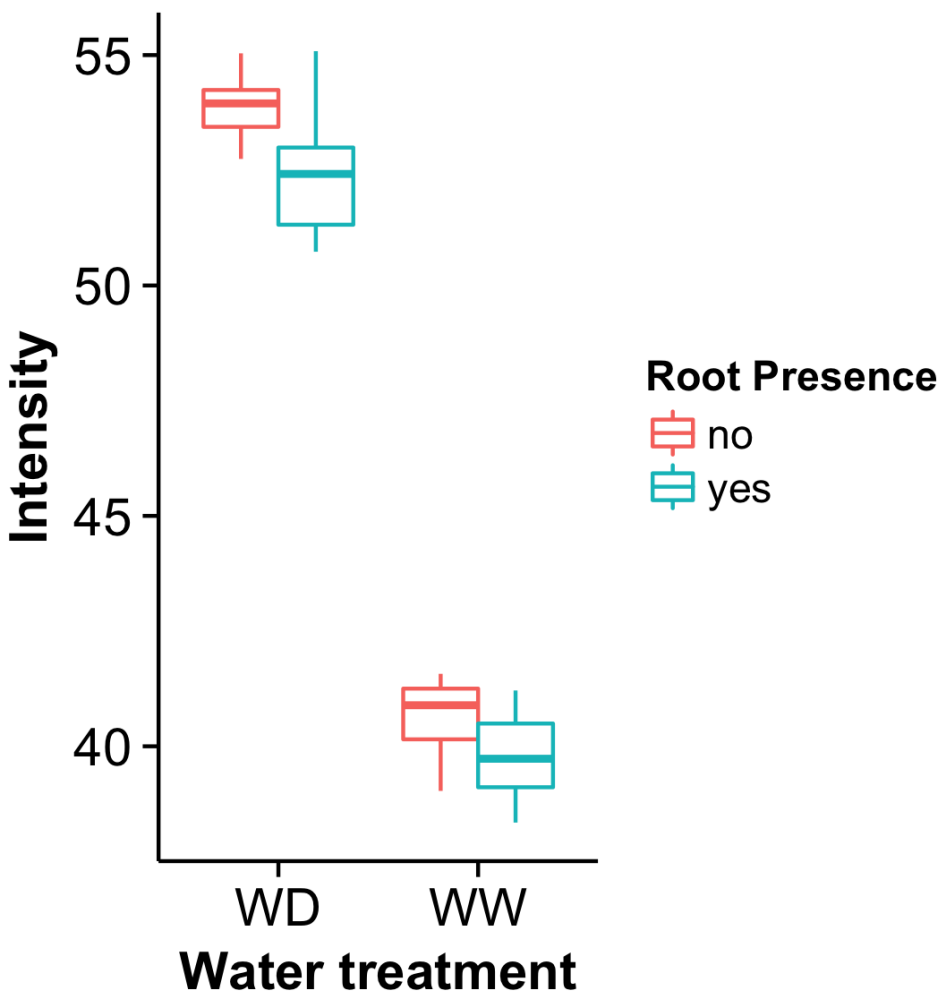
1172

1173 **Figure 9-Supplement 14-figure supplement 4. Three-reporter-based analysis of**
 1174 **root-root-microbe interactions. Plots showing output of directionality analysis**

1175 performed at different depths (0-5, 5-10, 10-15 cm) in rhizotrons exposed to
1176 light or kept in the dark. (0° is the direction of the gravity vector) A) Image
1177 showing a 22 DAS *ProUBQ10:LUC2o* plant (magenta) grown in the same
1178 rhizotron with *ProACT2:PpyRE8o* plants (grey). Plants were inoculated with
1179 *Pseudomonas fluorescens* CH267 (green). Magnified portion of root systems
1180 colonized by *Pseudomonas fluorescens* showing *P. fluorescences* (B) only or all
1181 three reporters together (C).

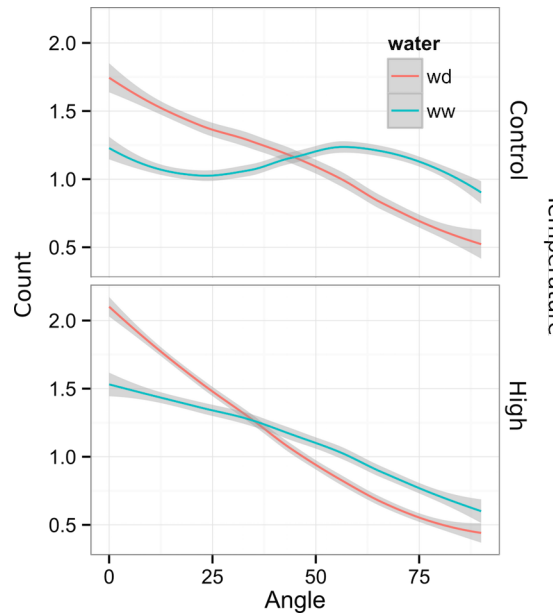


1182
1183 Figure 10 Supplement 5-figure supplement 1: Moisture calibration curve. Rhi-
1184 zotrons with different levels of moisture were prepared and scanned to obtain
1185 readings of pixel intensity. Soil from rhizotrons was then weighed, dried down
1186 in an oven at 70°C for 48 hours and percent water content quantified.

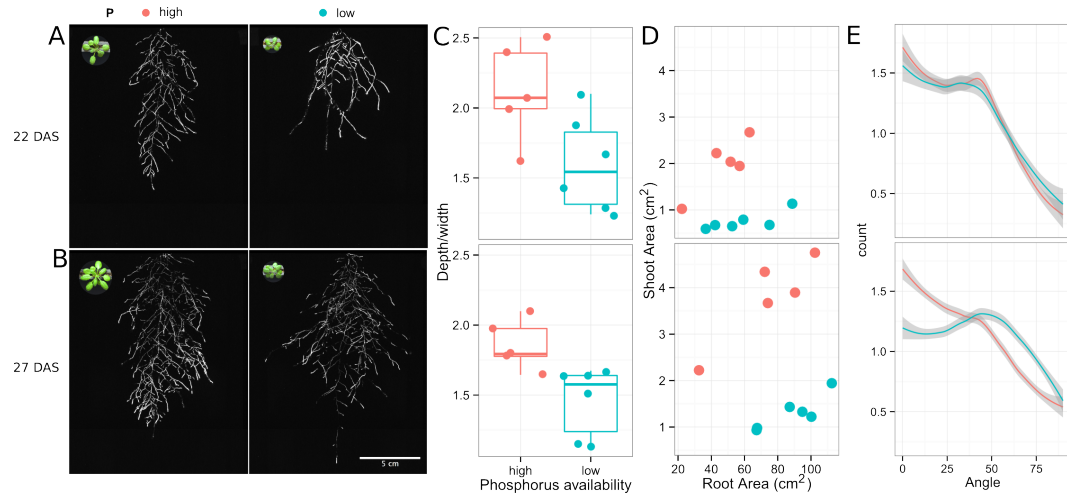


1187

1188 Figure 11—Supplement 15-figure supplement 2. Comparison of soil intensity
 1189 values between areas of the rhizotron with or without the presence of roots,
 1190 determined based on luminescence data. Mean intensity values from 100 x 100
 1191 pixel squares samples of both areas were obtained from 10 different rhizotrons.
 1192 Wilcoxon test analysis with $p < 0.01$ was used to test significant differences
 1193 between areas with or without root presence.

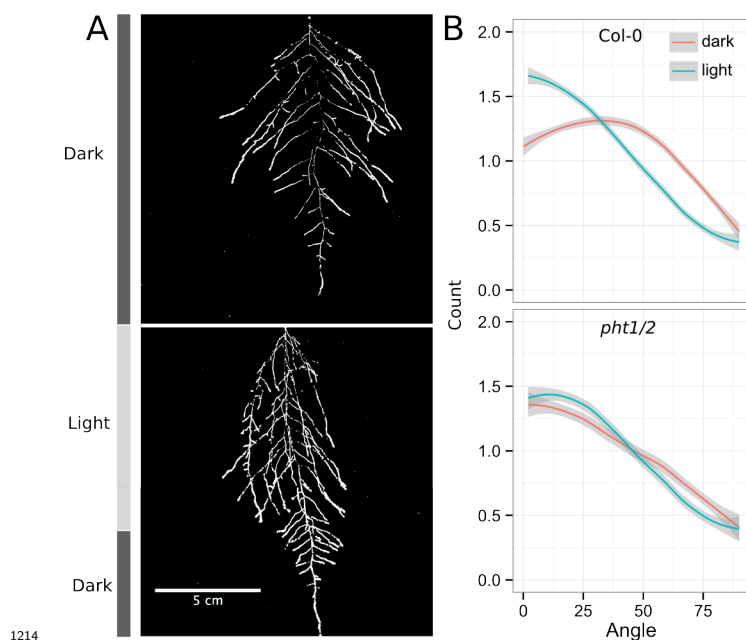


1194
1195 **Figure 6-figure supplement 1** Directionality analysis of roots of plants trans-
1196 ferred to water deprivation conditions after 9 DAS and kept 22 °C (control
1197 temperature) and 29 °C (high temperature) until 22 DAS. (0° is the direction
1198 of the gravity vector).



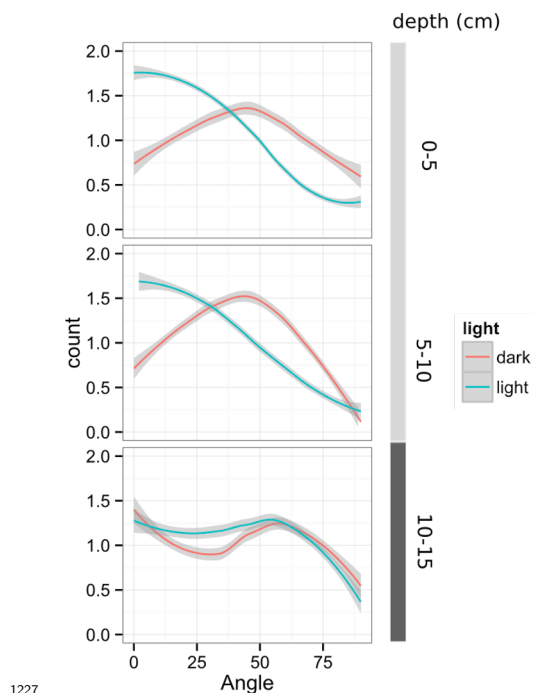
1199
1200 **Figure 11-Supplement 26-figure supplement 2. Phosphorus deficiency response**
1201 **of root systems Leaf relative water content of 23 DASplants that were**
1202 **subjected to water deprivation (ww) after 9 or 13 DAS or kept under well**

1203 **watered (ww)conditions.** Shoot and root systems of *ProUBQ10:LUC2o* Col-0
 1204 plants growing in soil supplemented with 1ml of 100 μ M P-Alumina (left) and
 1205 0-P-Alumina (right) 22 (A) or 27 (B) DAS. C) Root depth/width ratio of
 1206 22 (top) and 27 (bottom) DAS plants. D) Scatter-plot showing relationship
 1207 between root and shoot system area at 22 (top) and 27 (bottom) DAS. E) Root
 1208 directionality distribution in plants 22 (top) and 27 (bottom) DAS. Anova
 1209 analysis at $p < 0.01$ was used to compare depth/width ratios in P treatments.
 1210 Kolmogorov-Smirnov test at $p < 0.001$ was used to compare directionality
 1211 distributions between the different treatments. A Local Polynomial Regression
 1212 Fitting with 95% confidence interval (grey) was used to represent the
 1213 directionality distribution curve.(0° is the direction of the gravity vector).

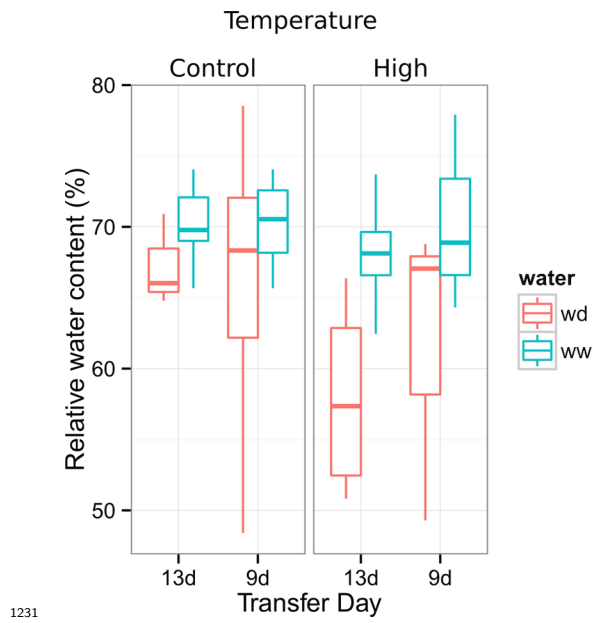


1214
 1215 **Figure 6-figure supplement 3. Effect of light on root directionality.** A) Col-0
 1216 root systems shielded (top) or light exposed (bottom). After 9 DAS the top
 1217 third of the rhizotron was exposed to light (indicated on the side with a light
 1218 grey bar) and plants were imaged at 20 DAS. B) Directionality analysis of
 1219 root systems shielded (red) or exposed (green) to light for Col-0 (top panel) or
 1220 *pht1/2* double mutant (bottom panel). Between 4 and 6 plants were analyzed

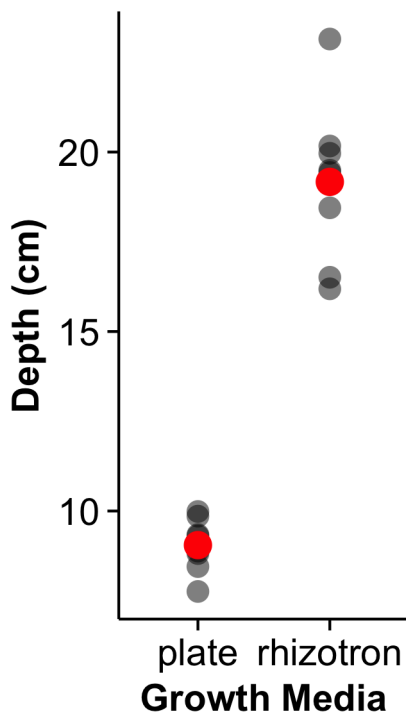
1221 per treatment. ANOVA analysis at $p < 0.01$ was used to compare depth/width
1222 ratios in P treatments. Kolmogorov-Smirnov test at $p < 0.001$ was used to
1223 compare directionality distributions between the different treatments. A Local
1224 Polynomial Regression Fitting with 95% confidence interval (grey) was used to
1225 represent the directionality distribution curve.(0° is the direction of the gravity
1226 vector).



1227
1228 **Figure 6-figure supplement 4** Plots showing output of directionality analysis
1229 performed at different depths (0-5, 5-10, 10-15 cm) in rhizotrons exposed to
1230 light or kept in the dark. (0° is the direction of the gravity vector).



1231
 1232 **Figure 6-figure supplement 5. Leaf relative water content of 23 DAS plants that**
 1233 **were subjected to water deprivation (WD) after 9 or 13 DAS or kept under well**
 1234 **watered (WD) conditions.** At 9 DAS half of the plants were kept under control
 1235 **temperature conditions** (22 °C) and the other half transferred to a 29
 1236 °C (high) chamber. n = 6-8 plants.



1237
1238 **Figure 8-figure supplement 1 Depth of the primary root of *Brachypodium* plants**
1239 **grown in rhizotrons or on gel-based media (n=8-11).**

1240 **Supplementary material**

1241 **Supplemental Material 1**

1242 Blueprints of the holders, clear sheets and spacers needed to built the rhizotrons.
1243 Additional details are provided in the materials and methods. Files are provided
1244 in Adobe Illustrator .ai and Autocad .dxf formats.

1245 **Supplemental Material 2**

1246 Primers used in the qPCR experiment.

1247 **Supplemental Material 3**

1248 Vector maps of all the constructs used in this work.

1249 [Source data files](#)

1250 [Source data files used for building the following figures are provided:](#)

1251 [figure_1D.csv](#)
1252 [figure_1_figure_supplement_1A-B.csv](#)
1253 [figure_1_figure_supplement_1C_D.csv](#)
1254 [figure_1_figure_supplement_1E-F.csv](#)
1255 [figure_1_figure_supplement_2.csv](#)
1256 [figure_1_figure_supplement_3.csv](#)
1257 [figure_2C.csv](#)
1258 [figure_2D.csv](#)
1259 [figure_3D.csv](#)
1260 [figure_3E.csv](#)
1261 [figure_3F-G_1.csv](#)
1262 [figure_3F-G_2.tps](#)
1263 [figure_3_figure_supplement_1A-B.csv](#)
1264 [figure_4G_reporter.csv](#)
1265 [figure_4G_root_segment.csv](#)
1266 [figure_4_figure_supplement_1.csv](#)
1267 [figure_4_figure_supplement_2.csv](#)
1268 [figure_5_figure_supplement_1.csv](#)
1269 [figure_6_A-D.csv](#)
1270 [figure_6_figure_supplement_2-C-D.csv](#)
1271 [figure_6_figure_supplement_2-E.csv](#)
1272 [figure_6_figure_supplement_3.csv](#)
1273 [figure_6_figure_supplement_4.csv](#)
1274 [figure_6_figure_supplement_5.csv](#)
1275 [figure_7.csv](#)
1276 [figure_8_figure_supplement_1.csv](#)

1278 **References**

- 1279 1.Dinneny, J. R. *et al.* Cell identity mediates the response of *Arabidopsis* roots
1280 to abiotic stress. *Science* 320, 942–945 (2008).
- 1281 2.Duan, L. *et al.* Endodermal ABA Signaling Promotes Lateral Root Quiescence
1282 during Salt Stress in Arabidopsis Seedlings. *Plant Cell* 25, 324–341 (2013).
- 1283 3.Lynch, J. P. & Wojciechowski, T. Opportunities and challenges in the subsoil:
1284 pathways to deeper rooted crops. *J. Exp. Bot.* 66, 2199–2210 (2015).
- 1285 4.Brady, N. C. & Weil, R. R. *Elements of the nature and properties of soils*.
1286 (Prentice Hall, 2009).
- 1287 5.Bao, Y. *et al.* Plant roots use a patterning mechanism to position lateral root
1288 branches toward available water. *Proc Natl Acad Sci* 111, 9319–9324 (2014).
- 1289 6.Tabata, R. *et al.* Perception of root-derived peptides by shoot LRR-RKs
1290 mediates systemic N-demand signaling. *Science* 346, 343–346 (2014).
- 1291 7.~~Marschner, P. *Marschner's Mineral Nutrition of Higher Plants*. (Academic
1292 Press, 2012).~~
- 1293 8.Rosquete, M. R. *et al.* An Auxin Transport Mechanism Restricts Positive
1294 Orthogravitropism in Lateral Roots. *Current Biology* 23, 817–822 (2013).
- 1295 9.~~8.Uga, Y. *et al.* Control of root system architecture by DEEPER ROOTING
1296 1 increases rice yield under drought conditions. *Nat. Genet.* 45, 1097–1102
1297 (2013).~~
- 1298 10.~~9.Postma, J. A. & Lynch, J. P. The optimal lateral root branching density
1299 for maize depends on nitrogen and phosphorus availability. *Plant Physiol.* 166,
1300 590–602 (2014).~~

- 1301 11.Kellermeier, F 10.Hara-Miyauchi, C. et al. Analysis of the Root System
1302 Architecture of *Arabidopsis* Provides a Quantitative Readout of Crosstalk
1303 between Nutritional Signals. Bioluminescent system for dynamic imaging of
1304 cell and animal behavior. *The Plant Cell Biochem. Biophys. Res. Commun.*
1305 26 419, 1480–1496 (2014) 188–193 (2012).
- 1306 12.Giehl, R.F., Lima, J.E 11.Emami, S., Yee, M.-C. & Wirén, N. von. Localized
1307 iron supply triggers lateral root elongation in *arabidopsis* by altering the
1308 *AUX1*-mediated auxin distribution. Dinneny, J. R. A robust family of Golden
1309 Gate Agrobacterium vectors for plant synthetic biology. *Front. Plant Cell Sc.*
1310 244, 33–49 (2012) 339 (2013).
- 1311 13.Galvan-Ampudia, C. S 12.Hall, M. P. et al. Halotropism Is a Response of
1312 Plant Roots to Avoid a Saline Environment. Engineered Luciferase Reporter
1313 from a Deep Sea Shrimp Utilizing a Novel Imidazopyrazinone Substrate.
1314 *Current Biology ACS Chem. Biol.* 23 7, 1–7 (2013) 1848–1857 (2012).
- 1315 14.Geng, Y 13.Lobet, G. et al. A spatio-temporal understanding of growth
1316 regulation during the salt stress response in *Arabidopsis*. Root System Markup
1317 Language: toward a unified root architecture description language. *Plant*
1318 *Cell Physiol.* 25 167, 2132–2154 (2013) 617–627 (2015).
- 1319 15.Slovak, R. et al. A Scalable Open-Source Pipeline for Large-Scale Root
1320 Phenotyping of *Arabidopsis*. 14.Moreno-Risueno, M. A. et al. Oscillating
1321 gene expression determines competence for periodic *Arabidopsis* root branching.
1322 *Plant Cell Science* 26 329, 2390–2403 (2014) 1306–1311 (2010).
- 1323 16.Moore, C. R. 15.Miller, G. et al. High-throughput computer vision
1324 introduces the time axis to a quantitative trait map of a plant growth response
1325 — The plant NADPH oxidase RBOHD mediates rapid systemic signaling
1326 in response to diverse stimuli. *Genetics Science Signaling* 19 52, 1077–1086
1327 (2013) ra45 (2009).

- 1328 17.Yokawa, K., Kagenishi, T. 16.Haney, C. H., Samuel, B. S., Bush, J.
1329 & Baluška Ausubel, F. Root photomorphogenesis in laboratory-maintained
1330 *Arabidopsis* seedlings. M. Associations with rhizosphere bacteria can confer
1331 an adaptive advantage to plants. *Trends Plant Sci. Nature Plants* 18, 117–119
1332 (2013). 15051 (2015). doi:10.1038/nplants.2015.51
- 1333 18.Bucksch, A. et al. Image-based high-throughput field phenotyping of crop
1334 roots. *Plant Physiol.* 166, 470–486 (2014).
- 1335 19.Trachsel, S. 17.Mandoli, D. F., Kaeppeler, S. M., Brown, K. MFord, G.
1336 A., WALDRON, L. J., NEMSON, J. A. & Lynch, J. P. Shovelomics: high
1337 throughput phenotyping of maize (*Zea mays* L.) root architecture in the field.
1338 Briggs, W. R. Some spectral properties of several soil types: implications for
1339 photomorphogenesis*. *Plant Soil Cell Environ.* 3413, 75–87 (2011) 287–294
1340 (1990).
- 1341 20.Devienne-Barret, F., Richard-Molard, 18.Galen, C., Chelle, M., Maury,
1342 ORabenold, J. J. & Ney, B. Ara-Rhizotron: an effective culture system to
1343 study simultaneously root and shoot development of *Arabidopsis*. Liscum, E.
1344 Functional ecology of a blue light photoreceptor: effects of phototropin-1 on
1345 root growth enhance drought tolerance in *Arabidopsis thaliana*. *Plant Soil New*
1346 *Phytol.* 280173, 253–266 (2006) 91–99 (2007).
- 1347 21.Tracy, S. 19.Moni, A., Lee, A. Y., Briggs, W. R. et al. Quantifying the
1348 impact of soil compaction on root system architecture in tomato (*Solanum*
1349 *lycopersicum*) by X-ray micro-computed tomography. *Annals of Botany* 110,
1350 511–519 (2012).
- 1351 22.Grunewald, W. et al. Transcription factor WRKY23 assists auxin
1352 distribution patterns during *Arabidopsis* root development through local
1353 control on flavonol biosynthesis. *Proc Natl Acad Sci* 109, 1554–1559 (2012).
- 1354 23.Hara-Miyauchi, C. et al. Bioluminescent system for dynamic imaging of

- 1355 ~~cell and animal behavior.~~ & Han, I. S. The blue light receptor Phototropin 1
1356 ~~suppresses lateral root growth by controlling cell elongation.~~ *Biochem. Biophys.*
1357 *Res. Commun. Plant Biology* **419**, 188–193 (2012) 34–40 (2014).
- 1358 ~~24. Emami, S., Yee, M.-C. 20. Yokawa, K., Kagenishi, T. & Dinneny, J. R. A~~
1359 ~~robust family of Golden-Gate Agrobacterium vectors for plant synthetic biology.~~
1360 ~~Baluška, F. Root photomorphogenesis in laboratory-maintained *Arabidopsis*~~
1361 ~~seedlings. *Front. Trends Plant Sci.* **4** 18, 339–117–119 (2013).~~
- 1362 ~~25. Lindeboom, J. J21. Lobell, D. B. et al. A Mechanism for Reorientation~~
1363 ~~of Cortical Microtubule Arrays Driven by Microtubule Severing. Greater~~
1364 ~~Sensitivity to Drought Accompanies Maize Yield Increase in the U.S. Midwest.~~
1365 *Science* **342** 344, 1245533–1245533 (2013) 516–519 (2014).
- 1366 ~~26. Meijon, M., Satbhai, S. B., Tsuchimatsu, T. 22. Ort, D. R. & Busch, W.~~
1367 ~~Genome-wide association study using cellular traits identifies a new regulator~~
1368 ~~of root development in . Long, S. P. Limits on Yields in the Corn Belt. *Nat.*~~
1369 *Genet. Science* **46** 344, 77–81 (2013) 484–485 (2014).
- 1370 ~~27. 23. Pacheco-Villalobos, D. & Hardtke, C. S. Natural genetic variation of~~
1371 ~~root system architecture from *Arabidopsis* to *Brachypodium*: towards adaptive~~
1372 ~~value. *Philosophical Transactions of the Royal Society of London B: Biological*~~
1373 *Sciences* **367**, 1552–1558 (2012).
- 1374 ~~28. 24. Watt, M., Schneebeli, K., Dong, P. & Wilson, I. W. The shoot and root~~
1375 ~~growth of *Brachypodium* and its potential as a model for wheat and other cereal~~
1376 ~~crops. *Functional Plant Biol.* **36**, 960–969 (2009).~~
- 1377 ~~29. 25. Mann, D. G. J. et al. Gateway-compatible vectors for high-throughput~~
1378 ~~gene functional analysis in switchgrass (*Panicum virgatum L.*) and other mono-~~
1379 ~~cot species. *Plant Biotechnol. J.* **10**, 226–236 (2012).~~
- 1380 ~~30. 26. Pacheco-Villalobos, D., Sankar, M., Ljung, K. & Hardtke, C. S. Disturbed~~
1381 ~~Local Auxin Homeostasis Enhances Cellular Anisotropy and Reveals Alternative~~

- 1382 Wiring of Auxin-ethylene Crosstalk in *Brachypodium distachyon* Seminal Roots.
- 1383 *PLoS Genet* 9, e1003564 (2013).
- 1384 31. Fang, S. et al. Genotypic recognition and spatial responses by rice roots.
- 1385 *Proc Natl Acad Sci* 110, 2670–2675 (2013).
- 1386 32. Haney, C. H., Samuel, B. 27. Buer, C. S., Bush, J. Ausubel, F. M. Associations
1387 with rhizosphere bacteria can confer an adaptive advantage to plants. *Nature*
1388 *Plants* 15051 (2015). doi:
- 1389 33. Moreno-Risueno, M. A. et al. Oscillating gene expression determines
1390 competence for periodic *Arabidopsis* root branching. *Science* 329, 1306–1311
1391 (2010).
- 1392 34. Miller, G. et al. The plant NADPH oxidase RBOHD mediates rapid systemic
1393 signaling in response to diverse stimuli. *Science Signaling* 2, ra45 (2009).
- 1394 35. Lynch, J., Brown, K. Snyder, R. Controlled release fertilizer comprising
1395 modified alumina having phosphorous bound to alumina surface. (2001). at
1396 ⇔
- 1397 36. Mandoli, D. F., FORD, G. A., WALDRON, L. J., NEMSON, J. A.
1398 Briggs, W. R. Some spectral properties of several soil types: implications for
1399 photomorphogenesis*Wasteneys, G. *Plant Cell Environ.* 13, 287–294 (1990).
- 1400 37. Galen, C., Rabenold, J. J. O. & Liscum, E. Functional ecology of a
1401 blue light photoreceptor: effects of phototropin-1 on root growth enhance
1402 drought tolerance in *Arabidopsis thaliana*. New Phyto~~Masle~~, J. Ethylene
1403 modulates root-wave responses in *Arabidopsis*. *Plant physiology* 173:132, 91–99
1404 (2007) 1085–1096 (2003).
- 1405 38. Moni, A., Lee, A. Y., Briggs, W. R. Han, I. S. The blue light receptor
1406 Phototropin 1 suppresses lateral root growth by controlling cell elongation.
1407 *Plant Biology* 34–40 (2014).

- 1408 39. Lobell, D. B. *et al.* Greater Sensitivity to Drought Accompanies Maize Yield
1409 Increase in the U.S. Midwest. *Science* 344, 516–519 (2014).—
- 1410 40. Ort, D. R. Long, S. P. Limits on Yields in the Corn Belt. *Science* 344,
1411 484–485 (2014).—
- 1412 41. 28. Blossfeld, S., Schreiber, C. M., Liebsch, G., Kuhn, A. J. & Hinsinger, P.
1413 Quantitative imaging of rhizosphere pH and CO₂ dynamics with planar optodes.
1414 *Annals of Botany* 112, 267–276 (2013).—
- 1415 42. 29. Shaw, S. L. & Ehrhardt, D. W. Smaller, Faster, Brighter: Advances in Op-
1416 tical Imaging of Living Plant Cells. [http://dx.doi.org/10.1146/annurev-arplant-](http://dx.doi.org/10.1146/annurev-arplant-042110-103843)
1417 042110-103843 64, 351–375 (2013).—
- 1418 43. López-Arredondo, D. L., Leyva-González, M. A., González-Morales, S.
1419 I., López-Bucio, J., Herrera-Estrella, L. Phosphate Nutrition: Improving
1420 Low-Phosphate Tolerance in Crops. *Annu. Rev. Plant Biol.* 65, 95–123 (2014).—
- 1421
- 1422 44. Lynch, J. P. Root phenes for enhanced soil exploration and phosphorus
1423 acquisition: tools for future crops. *Plant Physiol.* 156, 1041–1049 (2011).—
- 1424 45. 30. Grapov, D. DeviumWeb: Dynamic Multivariate Data Analysis and Visu-
1425 alization Platform.—
- 1426 46. 31. Branchini, B. R. *et al.* Red-emitting luciferases for bioluminescence re-
1427 porter and imaging applications. *Analytical Biochemistry* 396, 290–297 (2010).—
- 1428 47. 32. Branchini, B. R. *et al.* Thermostable red and green light-producing fire-
1429 fly luciferase mutants for bioluminescent reporter applications. *Analytical Bio-*
1430 *chemistry* 361, 253–262 (2007).—
- 1431 48. Hall, M. P. *et al.* Engineered Luciferase Reporter from a Deep-Sea Shrimp
1432 Utilizing a Novel Imidazopyrazinone Substrate. *ACS Chem. Biol.* 7, 1848–1857
1433 (2012).—

- 1434 49.33.Lane, M. C., Alteri, C. J., Smith, S. N. & Mobley, H. L. T. Expression of
1435 flagella is coincident with uropathogenic Escherichia coli ascension to the upper
1436 urinary tract. *Proc. Natl. Acad. Sci. U.S.A.* 104, 16669–16674 (2007).
- 1437 50.34.Ruegger, M. *et al.* The TIR1 protein of Arabidopsis functions in auxin
1438 response and is related to human SKP2 and yeast grr1p. *Genes Dev* 12, 198–207
1439 (1998).
- 1440 51.35.Moriwaki, T. *et al.* Hormonal Regulation of Lateral Root Development
1441 in Arabidopsis Modulated by MIZ1 and Requirement of GNOM Activity for
1442 MIZ1 Function. *Plant Physiol.* 157, 1209–1220 (2011).
- 1443 52.36.Vogel, J. & Hill, T. High-efficiency Agrobacterium-mediated transforma-
1444 tion of Brachypodium distachyon inbred line Bd21-3. *Plant Cell Rep* 27, 471–
1445 478 (2008).
- 1446 53.37.Covington, M. F. & Harmer, S. L. The Circadian Clock Regulates Auxin
1447 Signaling and Responses in Arabidopsis. *Plos Biol* 5, e222 (2007).
- 1448 54.38.Lobet, G. 38.Lindeboom, J. J. *et al.* Root System Markup Language:
1449 toward a unified root architecture description language. A Mechanism for
1450 Reorientation of Cortical Microtubule Arrays Driven by Microtubule Severing.
1451 *Plant Physiol. Science* 167342, 617–627 (2015)1245533–1245533 (2013).
- 1452 55.39.R Core Team. *R: A language and environment for statistical computing*.
1453 (R Foundation for Statistical Computing, 2014). at <<http://www.R-project.org/>
- 1454 org/>
- 1455 56.40.Wickham, H. *Tidyr: Easily tidy data with spread() and gather() functions*.
1456 (2014). at <<http://CRAN.R-project.org/package=tidyr>>
- 1457 57.41.Auguie, B. *GridExtra: Functions in grid graphics*. (2012). at <<http://CRAN.R-project.org/package=gridExtra>>
- 1458 58.42.Dryden, I. L. *Shapes: Statistical shape analysis*. (2013). at <<http://CRAN.R-project.org/package=shapes>>

- 1461 43. Adams, D. & Otarola-Castillo, E. Geomorph: An r package for the collection
1462 and analysis of geometric morphometric shape data. *Methods in Ecology and*
1463 *Evolution* 4, 393–399 (2013).
- 1464 44. Wickham, H. *Ggplot2: Elegant graphics for data analysis.* (Springer New
1465 York, 2009). at <<http://had.co.nz/ggplot2/book>>